TRITA-PFU-88-12

THREE-DIMENSIONAL MAGNETIC PROBE MEASUREMENTS OF EXTRAP T1 EQUILIBRIA

E. R. Hedin

TRITA-PFU-88-12

THREE-DIMENSIONAL MAGNETIC PROBE MEASUREMENTS OF EXTRAP T1 EQUILIBRIA

E. R. Hedin

Stockholm, December 1988

Department of Plasma Physics and Fusion Research
Royal Institute of Technology
S-100 44 Stockholm, Sweden

Three-Dimensional Magnetic Probe Measurements of Extrap T1 Equilibria

Eric R. Hedin

Department of Plasma Physics and Fusion Research
The Royal Institute of Technology
S-100 44 Stockholm

ABSTRACT

Internal probes are described for use in measuring the three orthogonal components of the magnetic field in the Extrap T1 device. The data analysis process for numerical processing of the probe signals is also explained. Results include radial and vertical profiles of the field components, three-dimensional field plots, inverse field strength contours, two-dimensional magnetic flux plots, and toroidal current profiles.

I. Introduction

Internal probes for measuring the three orthogonal components of the magnetic field in the Extrap T1 device are described. Extrap T1 [1] is a toroidal high-beta pinch plasma discharge experiment with major radius R = 0.45 m, and minor radius of the plasma current channel a ≈ 40 mm. Four conducting rings, external to the plasma current channel, each carry a peak current of approximately the same magnitude as the peak plasma current (20 - 30 kA). The combined magnetic field of the currents in the rings and plasma creates a square - shaped separatrix with x - points located near each ring. The plasma and ring currents are induced in parallel as the secondary of an iron - core transformer, which gives a discharge pulse length of ≈100 μsec. The plasma density, as measured by laser interferometry, is in the range n ≈ 0.5 to 1.0 X 10^{21} m^{-3}, varying with the hydrogen gas filling pressure. Thomson scattering yields an electron temperature T_e ≈ 10 to 35 eV, and toroidal flux loop and magnetic probe measurements yield poloidal average beta values of 20 to 60%.

II. Physical Description of the Probes

The dimensions of the probes were chosen to be as small as practicably possible in order to not perturb the plasma appreciably. The probe coils are enclosed in a 6 mm o.d. quartz tube, which when extended to the midplane blocks out only about 5% of the total plasma cross-section.

The probe consists of two sets of three orthogonally wound, interlocking coils. The two sets lie 2 cm apart on a cylindrical form of diameter 2.8 mm, made of PVC. Figure 1 shows a close-up photograph of the finished probe coils epoxied in place inside the 6 mm o.d. quartz tube. Enamel-coated copper wire of 0.1 mm diameter was used to give 18 turns in the windings through the holes, and 24 turns in the windings around the circumference of the cylindrical form. With these parameters, a typically encountered magnetic field variation, dB/dt, of 4 T/ms produces a voltage of ≈1.3 V across the output

of the coil, which if terminated in to 50 Ω, gives an L/R response time of ≈45 nsec. In order to maintain the signal size, active integrators (100 μsec time constant) are used which convert the coil output voltage to a signal proportional to B. The resulting signals are digitized and stored as data files on the LSI-11 computer dedicated to the Extrap experiments.

The quartz tube housing the probe coils is cemented to a stainless steel tube which passes out of the vacuum vessel and is attached to a positioning apparatus which allows complete rotation and vertical displacement of the probe. Figure 2 shows the probe and positioning apparatus mounted on a sector of the stainless steel toroidal vacuum vessel. As can be seen in Fig. 2, the quartz tube has two bends in it which give the probe a 28 mm swing radius when the quartz tube is rotated about its long axis. Four ports in the top lid of the vacuum vessel are available for mounting the probe at different major radii (R = 380, 430, 480, 530 mm).

The area accessible for measurement by the probes extends from R = 352 mm to R = 558 mm, and z = -75 mm to z = 85 mm. (Compare the inner dimensions of the vacuum vessel: 350 mm < R < 600 mm, and -90 mm < z < 100 mm.) The plasma current channel lies within the square shaped supports of the conducting rings (open area = 130 mm X 130 mm centered at R = 450 mm, z = 0 mm). Thus the probes can access the whole plasma cross-section as well as some area outside the ring supports. At present, two identical, complete probes have been made and mounted at the R = 480 mm and R = 530 mm ports.

A method of checking the influence of the probes on the plasma is to compare the plasma current with the probes fully extended into the current channel to the current when they are removed. This test revealed no discernable difference in plasma current for these two cases. Also, other experiments have shown that similarly constructed probes can be safely used under more severe plasma conditions than found in Extrap T1 [2-3].

III. Calibration Procedure and Data Reduction Techniques

In order to measure the magnetic field in an experiment such as Extrap T1, the standard procedure is to use one or a series of single magnetic pickup coils. The requirement for being able to employ such coils to obtain useful information on a particular component of the magnetic field (B_r, B_ϕ, or B_z) is that they must be precisely aligned with the component desired to be measured. Only one field component can be measured at a time, and even by rotating the coil perpendicular to its axis, at most two components of a three - dimensional field can be accessed.

In order to overcome these limitations, the three-dimensional probes described in this paper were designed. In using such probes, their relative position must still be accurately known, but precise alignment of a given coil with a certain field component is no longer a requirement. And no matter how the probes are placed, it becomes possible to obtain all three components of the magnetic field simultaneously at the location of the probe cluster.

The key to this capability is a calibration of the alignment of each coil axis with respect to some reference (typically the quartz tube housing), and the sensitivity of each coil to a given dB/dt. A stripline apparatus was built to provide a uniform magnetic field of known strength for the purpose of this calibration. By placing the probes in three different orthogonally oriented positions within the uniform field of the stripline and recording the integrated output signals, a 3 X 3 matrix of values (the "calibration matrix") for each three-coil, 3-D cluster can be built up. This matrix of values then forms the basis for unravelling the probe signals into the three components of the magnetic field. With the calibration matrix stored as part of a computer program, the analyzed field components can in principle be graphically displayed versus time almost immediately after a discharge. Appendix A provides a detailed description of the entire probe data collection and analysis procedure.

IV. Results and Discussion

The results presented in this section are intended as an example of the capabilities of the 3-D probe system, while also providing a collection of information pertaining to a certain standard operating regime of Extrap T1. In most instances, the results from vacuum shots and plasma discharges (8 mtorr hydrogen filling pressure) will be compared. Unless stated specifically otherwise, the data presented correspond in time to the peak of the main plasma current pulse (t = 2290 μsec). At this time, the measured plasma current is $I_{pl} \approx 20$ kA, and the inner ring currents are $I_{1,2} \approx 14.2$ kA, and the outer ring currents are $I_{3,4} \approx 5.8$ kA. At the same time for a vacuum shot, we have $I_{1,2} = 18.0$ kA, and $I_{3,4} = 11.8$ kA. A supplement included at the end of this report contains figures taken from a probe scan covering the whole plasma and ring system minor cross-section.

To start with, we show in Fig. 3 the three field components B_r, B_ϕ, B_z versus time for vacuum (top) and plasma (bottom) cases. We use a cylindrical coordinate system for labeling the field components, where in reference to the toroidal Extrap T1, z is up and r points in the direction of increasing major radius. The toroidal field starts at t = 1100 μsec and has a quarter period rise time of 1.1 ms, and the vertical field begins at t = 700 μsec with a 2.2 ms rise time. Both of these externally applied fields must soak through the vacuum vessel and ring/support mesh before building up in the plasma region [4]. But on the 100 μsec time scale of the main plasma current pulse, they are essentially constant, as the vacuum B_ϕ of Fig. 3 shows.

The capacitor bank which drives the induced plasma and ring currents is triggered at t = 2115 μsec. With the parameters used, the main plasma current pulse begins to build up at t ≈ 2200 μsec (as shown by an internal rogowski coil of inner radius r ≈ 60mm). The ionization and plasma build-up processes in Extrap T1 depend heavily on the internal field strength and filling pressure, and have been studied in Ref. [5].

In comparing B_ϕ for the vacuum and plasma cases, it is obvious that the plasma current has poloidal component in a direction so as to produce a paramagnetic response. The peak of this response corresponds in time to the peak of the plasma current pulse.

The next two figures show a sampling of the profiles obtained from 34 probe positions (one plasma and one vacuum shot at each position). In order to assemble these profiles, satisfactory shot-to-shot reproducibility must be guaranteed. The main acceptance criterion for a given discharge was that the peak plasma current should lie within a given range (19 - 22 kA). Also, occasional repeated discharges with a fixed probe position were measured and compared to show good reproducibility.

In Fig. 4 we plot the three field components versus z (z = 0 defines the equatorial midplane of the torus) at two different radial positions (R = 452 mm and R = 480 mm). B_z at R = 480 mm shows the pronounced influence of the outer octupole rings, located at R = 505 mm, z = ± 55 mm. At the time of these data, both the plasma and octupole ring currents flow in the minus toroidal direction.

In observing the vacuum radial field, (as well as the vacuum vertical field in Fig. 5) one sees the rather extended low-field region near the minor axis of the toroid. Also apparent is the approximate r^3 dependence of the magnetic field strength as calculated for a vacuum octupole field [6]. Upon comparing the vacuum and plasma toroidal field plots, the paramagnetic effect of the plasma is again evident.

Figure 5 contains profiles versus R of B_r, B_ϕ, and B_z for the vacuum and plasma cases at z = 0 mm and ±20 mm. In these profiles, two different probe sets were used, one mounted at R = 480 m, and one mounted at R = 530 mm. The outer set was used for measurements between R = 505 mm and R = 536 mm. Slight differences in the calibrations of these two probe sets can explain the small step at R = 505 mm in the radial profiles of the toroidal field.

In Fig. 6 we show three-dimensional plots of B_r and B_z, covering the outer half of the minor cross section, for vacuum and plasma cases. The individual line profiles of

Figures 4 and 5 comprise part of the data used in forming the 3-D mesh of field values in Fig. 6. Initially, a sparser mesh (approximately one half the mesh density shown in Fig. 6) is superimposed on the original, non-regularly spaced data points, and an interpolation routine is used to construct a regular matrix of data values at each grid point. Then a second application of the interpolation routine on the result of the first application yields the denser mesh of values plotted in Fig. 6. Line profiles of B_r and B_z extracted from the 3 - D mesh were demonstrated to closely reproduce the profiles made from only the original data points. However, a great advantage is gained by having the capability of interpolating the field values to a regular mesh. First, one avoids having to place the probes only at specified, regular grid points when collecting the data, and second, numerical data analysis (which requires regularly spaced data points) becomes possible.

Comparing the vacuum and plasma B_z plots of Fig. 6, it is apparent that the field from the two outer rings is substantially stronger for the vacuum case. This is an effect due to the difference in inductance of the ring system when plasma is present. The outer two rings are most markedly affected, and carry roughly one half as much current at the time of the plasma current maximum as they carry at that time without a plasma. Thus it is not possible to simply subtract the vacuum fields from those of a plasma discharge to obtain the plasma current contribution alone.

Using the values of B_r and B_z at each grid point, and forming |B| = sqrt(B_r**2 + B_z**2), then taking 1./(sqrt(|B| + .0001), where |B| is in Tesla, we obtain a matrix of values which can be given to a contour plotting routine. The result is shown in Fig. 7 for two different times of a plasma discharge. At t = 2305 μsec (15 μsec after the peak of the plasma current pulse), the plasma current is I_{pl} = 14.6 kA, the inner ring currents are $I_{1,2}$ = 18.0 kA, and the outer ring currents are $I_{3,4}$ = 9.8 kA. In both plots of Fig. 7, the higher density regions of contour lines correspond to areas of weak poloidal magnetic field. These are seen to be localized approximately at the center of the plasma current channel, and on the legs of the triangle between the plasma current channel and the two

outer rings. These two outer weak field regions correspond to the x - points which define the corners of the square-shaped separatrix formed by the combination of the fields from the plasma current and the octupole ring currents. It can be seen that at t = 2290 μsec, when the plasma current is much larger than the outer ring currents, no well defined x - points are present. However, at t = 2305 μsec, when the plasma and ring currents are closer in value, the x - points indeed become apparent. It is noticed that a more well-defined x - point exists near the bottom ring, which could be due to the slight up-down assymmetry in the vacuum vessel and ring currents.

One of the major goals of the development of the 3-D probes described in this article is the production of magnetic flux surface plots. Using the regular matrix of B_r and B_z values already described, the poloidal flux function ψ can be calculated from the following formula:

$$\mathbf{B}_{pol} = \frac{1}{R}(\nabla\psi) \times \hat{e}_\phi$$

where $\mathbf{B}_{pol} = B_r\hat{e}_r + B_z\hat{e}_z$, and $\hat{e}_\phi$ is the unit vector in the toroidal direction. Lines of constant flux are then calculated and drawn to create an experimental flux plot such as shown in the top half of Fig. 8. For comparison, the lower half of Fig. 8 contains an analytically calculated flux plot [7] based on plasma and ring currents equivalent to the experimental case. Both plots show the closed flux lines around the plasma and ring currents, as well as the x - points at the corners of the separatrix. The magnetic axis here lies on the z = 0 plane, but is shifted out to R ≈ 478 mm. For the analytical flux plot calculation, the externally applied vertical field at the magnetic axis is taken to be 30 G, which matches the experimental value at this time and position. Also a poloidal beta of 0.5 was assumed.

From the experimental data, we have the capability of studying the evolution of the flux surfaces in time. In Fig. 9 we show samples of the flux plots every 10 μsec from t = 2285 μsec (approximately at the peak of the plasma current pulse) to t = 2235 μsec when the plasma current has nearly extinguished. Due to the higher resistivity of the plasma

current channel than the conducting rings, (which act almost purely inductive on the time scale of the experiment) a phase difference exists between the plasma and ring currents. Thus, as noted beside each flux plot in Fig. 9, the ring currents steadily increase as the plasma current decreases. This leads to a somewhat complicated evolution of the ratio of the octupole field strengths to the poloidal field of the toroidal plasma current. The net result, however, is a macroscopically stable plasma quasi-equilibrium.

In conjunction with the flux plots of Fig. 9, we should consider Fig. 10 which shows the horizontal and vertical positions of the magnetic axis versus time. From Fig. 10a it is apparent that the plasma current channel begins well centered near the midpoint of the minor cross section, but then progressively moves outward to R ≈ 477 mm as the plasma current grows to its maximum value at t = 2290 μsec. At this point the outward motion is halted at the same time as the plasma current rather abruptly begins to decrease. (The primary loop voltage does not approach zero until t = 2320 μsec). This could perhaps indicate that the outer frame of the square-shaped ring supports (edge at R = 515 mm) has begun to act as a limiter. As the plasma current grows and moves outward, it eventually finds the outer portion of its channel blocked, which restricts further growth of the current. A larger externally applied vertical field B_v can help to offset the outwardly directed toroidal hoop force, **J X B**, but with increasing B_v comes greater difficulty in achieving initial breakdown of the plasma. However, recent improvments in the Extrap T1 preionization system should allow successful operation at higher values of B_v.

Comparing the radial velocity of the magnetic axis ($\approx 10^5$ cm/s) with the Alfven velocity ($\approx 10^7$ cm/s), we see that the plasma motion is slower by a factor of 100. This also indicates the stability of the Extrap T1 equilibrium to a class of instabilities with growth times on the order of the poloidal Alfven transit time. For non-circular plasma cross sections, however, axisymmetric unstable modes can exist which imply unbalanced forces on the plasma current, causing the plasma to move toward a minimum in the poloidal field [8]. The growth rate of these modes is typically on the order of the L/R time

of the conducting wall structure, or the L/R decay time of the plasma. For Extrap T1, the octupole rings and their supports form a conducting mesh around the plasma current channel. These conductors have a toroidal current L/R time of 1 ms, and a poloidal current L/R time of 150 μsec. The plasma's inductance and resistivity constantly change in time due to its varying cross-sectional size and temperature. But taking some average values, we estimate a plasma L/R time of 100 μsec. As is evident from Figures 9 and 10, no vertical instability of the plasma equilibrium occurs in the approximately 100 μsec long pulse length of the plasma current. In this time, an axisymmetric unstable mode should have had time to develop if indeed the Extrap T1 equilibrium was susceptible to it.

We now turn our attention to the calculation of the plasma current density as derived from Ampere's law $\mathbf{J} = (\nabla \times \mathbf{B})/\mu_o$. Considering only the toroidal component of $\mathbf{J}$, we can derive $\mu_o J_\phi = \partial B_r/\partial z - \partial B_z/\partial r$. Since we measure B_r and B_z over a major part of the plasma cross section, it becomes in principle a straightforward task to obtain a matrix of J_ϕ values. Taking derivatives of experimental profiles can lead to accentuated uneveness in the result, but with the intepolated mesh of field values available through the analysis of the probe measurements, satisfactory current density profiles are obtained. Figures 11 and 12 show radial and vertical profiles of the toroidal plasma current density at two different times. In Fig. 11, we have the profiles at t = 2290 μsec, with the vertical profiles at major radii R = 466 mm and R = 473 mm, and the radial profiles at Z = 0.5 mm and 8.5 mm. From these plots, it can be seen that the current density maximum lies at R ≈ 475 mm, and z ≈ 8.0 mm, which agrees well with the magnetic axis position at t = 2290 μsec, shown in Fig. 10. The next figure contains the same profiles at t = 2270 μsec, when I_{pl} = 15 kA, and the ring currents are passing through zero as they oscillate from flowing antiparallel to parallel to the plasma current. The unusual structure in the radial profiles of Fig. 11 is believed to be more than an artifact of the data analysis since upon calculating these J_ϕ profiles from the vacuum data yields relatively straight lines centered at $J_\phi = 0$. Further analysis of the radial plasma current density profiles reveals that the

minimum in J_ϕ at R = 487 mm exists for other z positions as well, but that the increased current density at R > 487 mm is localized around z = 8.5 mm, and diminishes substantially away from this point. Looking again at Fig. 12b, one observes that the current density turns towards zero at R = 515 mm, corresponding to the vertical edge of the ring supports, which acts as a limiter to the plasma current channel. Checking the radial J_ϕ profiles at other times shows that this two-lobed structure of the current density exists from the very beginning of the current pulse, and is most pronounced at about t = 2270 μsec. Thereafter, as the total plasma current continues to grow, the two channels merge into one, as can be seen in Fig, 11b. This single current channel persists as the total plasma current diminishes after t = 2290 μsec.

V. Summary

The three-dimensional probes described in this paper have enabled magnetic field measurements over a large part of the total plasma cross section yielding a more complete picture of the Extrap T1 equilibrium than has been available before. The data base consisting of B_r, B_ϕ, and B_z versus time and position is available for detailed analysis of the field spatial structure and its time dependence. Further analysis of the data has shown that magnetic flux surfaces can be formed which correspond closely to those obtained numerically. The time development of these flux surfaces reveals no macroscopic instabilities of the equilibrium on the time scale of the experiment. Calculation of the toroidal plasma current shows the formation of a well-defined current channel centered at the position of the magnetic axis.

VI. Supplement

A more recent probe scan covering the whole plasma and ring-system minor cross-section has yielded further data on the Extrap T1 equilibrium. For this scan, the filling pressure was 4 mtorr, and the average peak plasma current $I_{pl} = 28$ kA. The data was analyzed in the same manner as described in sections III and IV, and is presented in Figures 13 - 17.

Figure 13 shows radial and vertical profiles of the three components of the magnetic field at different z and R positions at time t = 2290 μsec (corresponding to the peak of the plasma current pulse). Figure 14 shows the inverse field strength plotted at six different times during the main plasma current pulse. The areas with concentrated field lines correspond to weak field regions. At times t = 2300 μsec and 2315 μsec, the four x - points surrounding the plasma current channel are visible. In Fig. 15, we plot six magnetic flux surfaces, following their evolution as the plasma current builds up, passes through its maximum, and gradually disappears. At time t = 2270μsec, the octupole ring currents pass through zero, from anti-parallel to co-parallel to the plasma current. Thus, at this time, the equilibrium resembles a normal z-pinch. No macroscopic instabilities are observed even during this period when the plasma current greatly exceeds the ring currents. Table 1 gives the values of the inner and outer ring currents as well as the plasma current at the times plotted in Figures 14 and 15.

In Fig. 16, vertical and radial profiles of the toroidal current density are exihibited at five different times. For the vertical profiles, the radii of the curves plotted correspond to the maximum radial position of the current density at that time (457 mm $\leq R_{max} \leq$ 461 mm). Figure 17 shows 3-D plots of the toroidal current density at two times: t = 2225 μsec (before the plasma current pulse begins), and t = 2290μsec (at the peak of the plasma current pulse -- note that the ring currents have now changed direction).

TABLE 1

Plasma and Ring Currents at Selected Times

	time (μs)	$I_{1,2}$(kA)	$I_{3,4}$(kA)	I_{pl}(kA)	
	2225	-32	-20	0	
	2260	-5	-5	15	
	2270	3	0	24	
	2290	15	7	28	
	2300	17	9	26	
	2315	20	11	13	
	2325	21	12	8	
	2340	23	13	0	

REFERENCES

[1] DRAKE, J.R., BRUNSELL, P., BRZOZOWSKI, J., ENINGER, J.E., HEDIN, E.R., KARLSSON, P., LEHNERT, B., LI, JIN, SCHEFFEL, J., SÄTHERBLOM, H.E., TENNFORS, E. and WILNER, B., Experimental studies of a high-beta, noncircular cross-section, toroidal pinch, *Plasma Physics and Controlled Nuclear Fusion Research* 1988 (Proc. 12th Int. Conf. Nice, 1988) paper **IAEA-CN-50/**C-5-19.

[2] HEDIN, E.R., KOEPKE, M.E., and RIBE, F.L., Experimental Studies of the Equilibrium of a linear, high-beta l=1 stellarator, *Phys. Fluids* **30**, 2885 (1987).

[3] LIPSCHULTZ, B., PRAGER, S.C., TODD, A.M.M., and DELUCIA, J., Axisymmetric instabilities in a noncircular tokamak: experiment and theory, *Nucl. Fusion* **9**, 1509 (1979).

[4] BRUNSELL, P., LI, JIN, Royal Institute of Technology, Stockholm, TRITA-PFU-88-05.

[5] LI, JIN, Breakdown analysis for electrode-less discharge in a magnetic field, Royal Institute of Technology, Stockholm, TRITA-PFU-88-07.

[6] SCHEFFEL, J., Toroidal Extrap equilibrium, Royal Institute of Technology, Stockholm, TRITA-PFU-82-06.

[7] LI, JIN, Private Communication.

[8] LIPSCHULTZ, B., PRAGER, S.C., TODD, A.M.M., and DELUCIA, J., Axisymmetric instabilities in a noncircular tokamak: experiment and theory, University of Wisconsin, COO-2387-116 (1979).

APPENDIX A

Detailed Explanation of the 3-D Probe Data Acquisition and Analysis Procedure

I. Calibration Procedure

A stripline device of dimensions 0.147 m X 0.281 m X 0.035 m is used to provide an almost uniform field in the area between the parallel copper plates. Coaxial cables connect the stripline to a 3.91 μF capacitor which is charged to 15 kV to provide 12 - 13 kA of current at the first peak. The stripline and capacitor form an LC circuit with a frequency f ≈ 38 kHz.

Figure A1 shows a drawing of the stripline. The three slots (1-3) are 10.5 cm deep, and allow the quartz tube with the 3-D probes inside the tip to be inserted to the center of the stripline where the field is the most uniform. The probes should be inserted along the sides of the slots labelled"a" for each slot. With the probes inserted and connected to the data acquisition system as described in section III, two shots should be taken at each slot postition. It is also important to record on the computer the current through the stripline as measured by a current transformer which gives 0.005 V/amp when terminated into 50 ohms.

II. Mounting Procedure

The fully assembled probe and positioning apparatus must be aligned or zeroed to the proper angular position before mounting on the vacuum vessel. This is done by mounting the probe assembly on the specially constructed phenolic lid to the extra toroidal vacuum vessel sector. With the rotation stage set to 0 degrees, the quartz tube is rotated so that its tip (where the coils are located), points toward the large major radius side of the toroidal sector; then the locking bolts are drawn tight. A special consideration is required when the probe is to be mounted in positions 2 or 4 (numbered from the inside) on the lid of the vacuum vessel. Due to a manufacturing shortcoming, the mounting bolt holes for these two positions are rotated by 11.25 degrees with respect to the correct orientation as

on the phenolic lid. Thus a compensating 11.25 degree turn of the quartz tube must be made.

When mounting the assembled and aligned probe on the toroidal vacuum vessel, be aware that the octupole rings must avoided by turning the quartz tube appropriately via the rotation stage.

III. From Probe to Data File

Six thin coaxial cables (three for each of two 3-D probe sets) are numbered 1-6 and should be connected to the probe connection box according to Fig. A2. The other ends lead to the data panel where they should be connected to the variable attenuators, which should in turn be connected to the active integrators (RC = 100 μsec), whose outputs go to the opto links (with 50 ohm inputs). It is important to use the exact same integrators and opto links as were used for each probe line in the calibration procedure. The amount of attenuation required varies for each probe winding according to the orientation of the probes in the vacuum vessel, but factors of 2, 5, and at most 10 should be adequate. If these attenuators are used, their values must be entered by hand into the DAMPT program. Inside the screen room, connect the opto link outputs to the digitizers (the LeCroy 2256AS digitizers are most convenient since they have variable input attenuation which is read directly by the data acquisition program).

The DAMPT program must be set up in the following way in order to record data from the probes properly. First, type MOD HEA for each of the digitizer unit numbers, and set the units to "V" (the signal stored is in volts), and the scale factors to the value of external attenuation used. Next, the correct probe numbers must be entered in the header. In Fig. A2, one can see that the probe sets are labelled "bottom" and "top", referring to their orientation when placed in the vacuum vessel. Also, each winding is labelled 1, 2, or 3. So, if each cable from the probe connection box to the attenuators is connected as shown in Fig. A2, the following order is given for probe winding to cable number:

(probe winding) T1,T1,T3,B1,B2,B3 = 1,2,3,4,5,6 (cable number).

The probe number to be entered in the header consists of a 2-digit code. The first digit in the code refers to the radial positon of the probe axis as it is mounted on the lid of the vacuum vessel: 1 = 380 mm, 2 = 430 mm, 3 = 480 mm, 4 = 530 mm. The second digit in the code refers to the particular winding of the 3-D probes:

(probe winding) B1,B2,B3,T1,T2,T3 = 1,2,3,4,5,6 (second digit).

So, for example, if a probe assembly is mounted in the third position (R = 480 mm), the probe number code to be entered in the header of digitizer collecting data from winding B1 would be 31, and that for winding B2 would be 32, and so on. This information is used in the data analysis program BTRANS.

Next, the probes' positions must be entered in DAMPT; this is done via MOD PRO. The program will ask for a probe number, and any of probe numbers entered in the headers will suffice for an answer (31, for example). The information requested by the program is the probes' angular position and delta-z value. The angle is read off the rotation stage (in degrees), and the delta-z value (in mm) refers to the distance of the center of the bottom probe cluster above (positive z) or below (negative z) the equatorial midplane. Once entered, this data is stored automatically in the headers of all the probes with the same first digit in their codes. SHO PRO can be used to check the current values of angle and delta-z.

To perform data analysis of the probe signals, the probe data files must be transferred to the QZ DEC-10 computer. This is done in the followi ıg way. On the data acquisition computer, run the program GETFIL to prepare the files to be transferred to QZ. Next, run KERMIT to perform the file transfer. A brief description of how to transfer files with KERMIT is given here. The responses typed by the user are printed in italics.

.KERMIT (Note: the period"." must also be typed)

KERMIT-11>*CONN TT5:*

KTHNET->*QZ-DEC*

login here to an account on QZ

KERMIT

KERMIT-10>*SERVER*

<CNTRL> \ *C* (this is control-backslash, then C)

KERMIT-11>*SEND DL1:[301,2]FILENAMES*

KERMIT-11>*FINISH*

KERMIT-11>*EXIT*

Explanatory notes: The program GETFIL stores the files it creates in directory DL1:[301,2]. TT5 is the label of the line connecting the data acquisition computer to KTHNET. In sending files, wildcards can be used (for example, 12999.*). After checking that the files have transferred properly, delete them from directory DL1:[301,2]. To get a file from the DEC-10 computer to the Extrap computer, type GET instead of SEND.

IV. Data Analysis Procedure

Several programs exist on the DEC-10 computer to carry out the analysis, plotting, and further reduction of the magnetic probe data. These build upon the raw data files transferred according the directions in the previous section. A step-by-step description of the procedure required to utilize these files is given in this section. Also given is an in-depth explanation of the analysis theory of 3-D probes.

1. From calibration data to MAGDAT file

When the probes are calibrated in the stripline device, they are placed consecutively in the three different slots labelled 1a, 2a, 3a. The resultant field directions with respect to the quartz tube containing the probes is shown in Fig. A3a. When the probe lies in slot 1a, the field is in the direction labelled B_{1a}, and so forth. Next, we need to consider the placement of the probes inside the vacuum vessel. Figure A3b shows a picture of the quartz tube oriented so as to point toward the toroidal major axis. In this orientation, the rotation stage should read 180 degrees; this is the angle α which is entered into the DAMPT program through the MOD PRO command.

The three field components shown in Fig. A3b correspond to the cylindrical coordinate system of the torus (r, ϕ,z), as well as the "probe coordinates" (α,β,γ) which have the quartz tube as their frame of reference. These two coordinate systems align with one another only when the probe is oriented as shown. If the quartz tube is rotated via the rotation stage, only B_z and B_γ remain aligned; the other two coordinate axes rotate as shown in Fig. A3d. The angle θ is not the same as the angle α, but they are related as shown in Fig. A3e. Here, d is as given in Fig. A3a (d = 28 mm), R_o is the major radius position of the long axis of the quartz tube (R_o = 380 mm, 430 mm, 480 mm, or 530 mm), R_p is the major radius position of the probe coils. The quantities R_o, d, and α are knowns, and the desired unknowns, R_p and θ, can be expressed in terms of them as follows:

$$R_p = \mathrm{sqrt}(R_o^2 + d^2 + 2dR_o\cos\alpha). \qquad \text{(A1)}$$

As an intermediate step, the angle γ is calculated:

$$\gamma = \arcsin\left(\frac{d}{R_p}\sin\alpha\right) . \qquad \text{(A2)}$$

And then,

$$\theta = \pi - \alpha + \gamma \qquad \text{(A3)}$$

These steps are carried out in the probe analysis program BTRANS.

Referring back to Fig. A3, we see that when the probe is in the stripline, we can write the output signals from a given winding (three orthogonal windings make up a probe set) as follows: For winding number B1, for example,

$$V_{1\alpha} = C_1 B_\alpha \cos\alpha_1 \ , \ V_{1\beta} = C_1 B_\beta \cos\beta_1 \ , \ V_{1\gamma} = C_1 B_\gamma \cos\gamma_1 \ , \qquad \text{(A4)}$$

where $V_{1\alpha}$ is the signal (in volts) from winding B1 when placed in slot 2a, $V_{1\beta}$ is the signal from slot 1a, and $V_{1\gamma}$ is the signal from slot 3a. C_1 is the "calibration factor" for winding B1; B_α, B_β, and B_γ are the peak field strengths when the probe is placed in slots 2a, 1a, and 3a, respectively; and $\cos\alpha_1$, $\cos\beta_1$, and $\cos\gamma_1$ are the "angle cosines" of the normal to the plane of the winding in probe coordinates (see Fig. A3c). For example, if γ = 0, the winding will only respond to a field component precisely aligned with the γ-

axis. During the calibration, the signals $V_{1\alpha}$, $V_{1\beta}$, and $V_{1\gamma}$ are recorded for all three windings of a 3 - D probe set.

The angle cosines have the property that

$$\cos^2\alpha + \cos^2\beta + \cos^2\gamma = 1, \qquad \text{(A5)}$$

so we can solve for C by the forming

$$C = \left[\left(\frac{V_\alpha}{B_\alpha}\right)^2 + \left(\frac{V_\beta}{B_\beta}\right)^2 + \left(\frac{V_\gamma}{B_\gamma}\right)^2 \right]^{.5} \qquad \text{(A6)}$$

In practice, B is the current in amps through the stripline at the time the signal V was measured. Once C is known, we find

$$\cos\alpha = \frac{V_\alpha}{CB_\alpha f_\alpha}\ ,\ \cos\beta = \frac{V_\beta}{CB_\beta f_\beta}\ ,\ \cos\gamma = \frac{V_\gamma}{CB_\gamma f_\gamma}\ . \qquad \text{(A7)}$$

The new quantities f_α, f_β, and f_γ introduced in the equation above are the factors by which the acutal field in the stripline differs from an ideal stripline. These factors are somewhat position dependent and can be calculated or measured (for example, see program PROBCAL on the data-acquisition computer). The field of an ideal stripline of width L is $B = \mu_o I/L$. For our stripline, L = 0.147 m, which implies that I/B = 117 kA/T, using the ideal formula.

Now we have sufficient information to write the file MAGDAT.DAT, which is an input file to the data analysis program BTRANS. The calibration factors for the windings should be typed as the first six lines of MAGDAT in the following order: B1, B2, B3, T1, T2, T3. These factors must have units [Volts/Tesla]. The next lines contain the angle cosines of the windings (same ordering), with one number per line. Enter the cosines in the order α, β, γ for each winding. It will be noticed when looking at Figures 4a and 4b that the directions B_{2a} and $B_{r,\alpha}$ are opposite to each other. This means that all the cosine alphas must have their signs reversed before entering them into MAGDAT.

With the MAGDAT.DAT file formed, we are now ready to analyze probe data files using the program BTRANS. BTRANS opens the file MAGDAT.DAT, and uses the calibration factors and angle cosines to transform the three signals in volts (stored in three

separate data files) from the three windings of a probe set into the three orthogonal field components B_r, B_ϕ, and B_z. For a field in an arbitrary direction at the position of the probe cluster,

$$B = B_\alpha \hat{e}_\alpha + B_\beta \hat{e}_\beta + B_\gamma \hat{e}_\gamma , \qquad (A8)$$

the integrated signal out from a given winding of the cluster is

$$V = C(B_\alpha \cos\alpha + B_\beta \cos\beta + B_\gamma \cos\gamma) . \qquad (A9)$$

Here, the coordinate directions (α, β, γ), called probe coordinates, are defined with respect to the quartz tube, as shown in Fig. A3b. Compiling the signals from each of the three windings of a cluster in matrix form, we have,

$$\begin{pmatrix} V_1/C_1 \\ V_2/C_2 \\ V_3/C_3 \end{pmatrix} = \begin{pmatrix} \cos\alpha_1 & \cos\beta_1 & \cos\gamma_1 \\ \cos\alpha_2 & \cos\beta_2 & \cos\gamma_2 \\ \cos\alpha_3 & \cos\beta_3 & \cos\gamma_3 \end{pmatrix} \begin{pmatrix} B_\alpha \\ B_\beta \\ B_\gamma \end{pmatrix} \qquad (A10)$$

or $\mathbf{V_c} = \underline{\mathbf{P}} \cdot \mathbf{B_p}$, where $\underline{\mathbf{P}}$ is the calibration matrix.

Next, we need the field in lab coordinates. For this, we require information on the position of the probe stem in the vacuum vessel; that is, what angle has the probe rotated about the z,γ - axis from the unique position where probe and lab coordinates coincide? From Fig. A3d, we see that we can write

$$B_r = B_\alpha \cos\theta + B_\beta \sin\theta$$

$$B_\phi = -B_\alpha \sin\theta + B_\beta \cos\theta , \qquad B_z = B_\gamma , \qquad (A11)$$

or in matrix form,

$$\begin{pmatrix} B_r \\ B_\phi \\ B_z \end{pmatrix} = \begin{pmatrix} \cos\theta & \sin\theta & 0 \\ -\sin\theta & \cos\theta & 0 \\ 0 & 0 & 1 \end{pmatrix} \begin{pmatrix} B_\alpha \\ B_\beta \\ B_\gamma \end{pmatrix} , \qquad (A12)$$

which is $\mathbf{B} = \underline{\mathbf{M}} \cdot \mathbf{B_p}$. From Eq. A10, $\mathbf{B_p} = \underline{\mathbf{P}}^{-1} \cdot \mathbf{V_c}$, which we insert in Eq. A12 to obtain

$$\mathbf{B} = \underline{\mathbf{M}} \cdot (\underline{\mathbf{P}}^{-1} \cdot \mathbf{V_c}) = (\underline{\mathbf{M}} \cdot \underline{\mathbf{P}}^{-1}) \cdot \mathbf{V_c} . \qquad (A13)$$

Thus, one can obtain the three laboratory coordinate components of an arbitrarily directed field. These three components of **B** are stored in separate new data files which BTRANS creates.

2. Data Storage

The capability of long term file storage exists through the QZ system. A separate brief report has been written describing the procedure to do this.

3. Plotting Capabilities

In order to plot the analyzed output files from BTRANS, the program MAGPLO should be used. This program reads a number of output files from BTRANS and plots them with typically three curves per plot, and two plots per page. It also creates an output file, called MAGOUT.DAT, which lists the magnetic field data at specified time intervals. An input file to MAGPLO must be created (called MAGLST.DAT) which lists the shot numbers or files names to be plotted and how many curves per plot. The specific format for MAGLST.DAT is described in comment statements in MAGPLO. The results from MAGPLO are curves of **B** versus time. The output file which MAGPLO creates will contain numbers corresponding to the magnetic field values of the curves plotted at 32 evenly spaced instants in time. This output file can be renamed and saved as the basis for further reduction and analysis of the data.

4. From Magnetic Fields to Flux Plots

The program FLUXPL contains most of routines used to further analyze the magnetic field data to create flux plots, calculate the toroidal current density, etc. Its only input file is MAGOUT.DAT as created by BTRANS, which should be renamed MAGFLX.DAT in order to be opened by FLUXPL. Options to the program FLUXPL are supplied by the user through replies to questions asked by the program at the terminal. These options include the following:

1. Input the number of R and z grid points. (A rectangular area, bounded by the most extreme of the data points, will be divided up into the specified number

of R and z grid points, which must be at most 20. This grid density will later in the program be automatically doubled).

2. Input NX,NY,WEIGHT for MDFMAT. (These values are parameters used by the DISSPLA routine MDFMAT in interpolating the data points to values at the regular grid points. See section 3.8 of the DISSPLA manual for details. NX = 2, NY = 2, WEIGHT = 7 yields reasonable results).
3. Select R, z range? (Refers to the limits for a data point read from file MAGFLX.DAT to be accepted).
4. If yes, input rmin, rmax, zmin, zmax in mm.
5. Calculate the position of the magnetic axis at various times?
6. If yes, input start and end times -- must be within the range of times included in the input file MAGFLX.DAT.
7. Make raw-data file RAWDAT.DAT? (This file will contain values of B_r, B_ϕ, and B_z at the analysis time chosen in question 3 for all the magnetic field data contained in MAGFLX.DAT).
8. Which analysis time? (Must be one of the times available in MAGFLX.DAT).
9. Input rmin, rmax, zmin, zmax. (These values are used in determining the limits of extrapolation when forming the interpolated mesh of field values).
10. Make flux plots?
11. If yes, input the number of contours.
12. Make magnetic field surface plots? (3 - dimensional).
13. Make magnetic field line plots? (3 - dimensional line plots).
14. Calculate and plot the toroidal current? (The plots will be both 3 - D as well as profile plots of J_{TOR} versus R or z).
15. (If any 3 - D plots are chosen, the following data will be requested):
    Input phi, theta, and radius for the viewing angle. (25.,25.,2. is a suitable reply here).

16. Make field profile plots? (This refers to B_r and B_z from the interpolated data mesh as plotted versus R or z. More specific information regarding these plots is asked by the subroutine at the time it is running).

17. Choose terminal screen or HP printer for displaying the plots.

To create flux plots, the flux function $\psi(R,z)$ is calculated from the interpolated mesh of poloidal field values in the following way. First, we form

$$\psi(R_o,z) = \psi(R_o,z_o) - \int_{z_o}^{z} R_o B_r(R_o,z)dz \,, \qquad \text{(A14)}$$

where R_o is the innermost radial position of the rectangular shaped R-z mesh of poloidal field values. The value $\psi(R_o,z_o)$ is set to 0 without loss of generality. Next we perform an integration in R using $\psi(R_o,z)$ as the constant of integration.

$$\psi(R,z) = \psi(R_o,z) + \int_{R_o}^{R} RB_z(R,z)dR \,. \qquad \text{(A15)}$$

In this manner, an R-z matrix of ψ values can be built up which is available for input to a contour plotting routine.

5. Non-interpolated field profiles

The output file RAWDAT.DAT from program FLUXPL can be used in conjunction with program RAWDAT to make profile plots of B_r, B_ϕ, and B_z versus R or z. From 1 to 6 curves per plot can be accomodated, and each curve will include every data point within a user specified range in R or z. Separate minimum and maximum limits on the y-axis (Tesla) can be specified for each of the three plots, or the computer can be made to choose reasonable limits.

FIGURE CAPTIONS

Fig. 1 Close-up photograph of the two three - dimensional probe sets inside the 6 mm o.d. quartz tube.

Fig. 2 Photograph of the probe and positioning apparatus mounted on a sector of the stainless steel troidal vacuum vessel.

Fig. 3 The three components of the Extrap T1 magnetic field versus time at R = 452 mm, z = 0.0 mm. (a) Vacuum fields (b) plasma discharge fields.

Fig. 4 Vertical profiles of the three components of the Extrap T1 magnetic field at major radii R = 452 mm and R = 480 mm. (a-c) Plasma discharge fields (d-f) vacuum fields.

Fig. 5 Radial profiles of the three components of the Extrap T1 magnetic field at z = -20 mm, 0.0 mm, and 20 mm. (a-c) Plasma discharge fields (d-f) vacuum fields.

Fig. 6 Three - dimensional magnetic field plots showing the vertical and radial components. (a,b) Plasma discharge fields (c,d) vacuum fields.

Fig. 7 Inverse field strength plots covering the outer half of the minor cross section for plasma discharges at (a) t = 2290 μsec (b) t = 2305 μsec.

Fig. 8 Magnetic flux surface plots corresponding in time to the peak of plasma current pulse (t = 2290 μsec). (a) Experimental, and (b) analytically based plots.

Fig. 9 Time evolution of the magnetic flux surfaces at 10 μsec intervals from t = 2285 μsec to t = 2335 μsec.

Fig. 10 Magnetic axis position versus time. (a) Radial position (b) vertcal position.

Fig. 11 Toroidal current density profiles for plasma discharges at t = 2290 μsec. (a) Vertical profiles at major radaii R = 466 mm and R = 473 mm. (b) Radial profiles at z = 0.5 mm and z = 8.5 mm.

Fig. 12 Toroidal current density profiles for plasma discharges at t = 2270 μsec. (a) Vertical profiles at major radaii R = 466 mm and R = 473 mm. (b) Radial profiles at z = 0.5 mm and z = 8.5 mm.

SUPPLEMENT

Fig. 13 Radial and vertical profiles of the three components of the Extrap T1 magnetic field at different z and R positions at time t = 2290 μsec.

Fig. 14 Inverse field strength plots covering the whole minor cross-section for plasma discharges at t = 2225 μsec, 2260 μsec, 2270 μsec, 2300 μsec, 2315 μsec, 2325 μsec.

Fig. 15 Magnetic flux surfaces of the whole minor cross-section for plasma discharges at t = 2260 μsec, 2270 μsec, 2300 μsec, 2315 μsec, 2325 μsec, t = 2340 μsec.

Fig. 16 Vertical and radial profiles of the toroidal current density at times t = 2270 μsec, 2280 μsec, 2290 μsec, 2300 μsec, 2315 μsec.

Fig. 17 Three-dimensional plots of the toroidal current density at times t = 2225 μsec, and t = 2290 μsec.

APPENDIX A

Fig. A1 Schematic drawing of the stripline apparatus.

Fig. A2 Drawing of the quartz tube housing the two three-dimensional probes. Winding labels showing the correspondence between the coils and the cables in the probe connection box are also shown.

Fig. A3 Diagrams illustrating the relationship of the probe to the various field directions. (a) Orientation of the probe to the stripline field when the probe is placed in slots 1a, 2a, and 3a. (b) Relationship between lab coordinates and "probe" coordinates when the probe is oriented so as to point toward the center line of the torus. (c) The three angle cosines of the normal to the surface of a probe coil, shown in probe coordinates. (d) Relationship between lab and probe coordinates when the probe is rotated around its long axis by an angle θ. (e) Relationships between various angles and lengths used in calculating the probe's position.

Fig.1

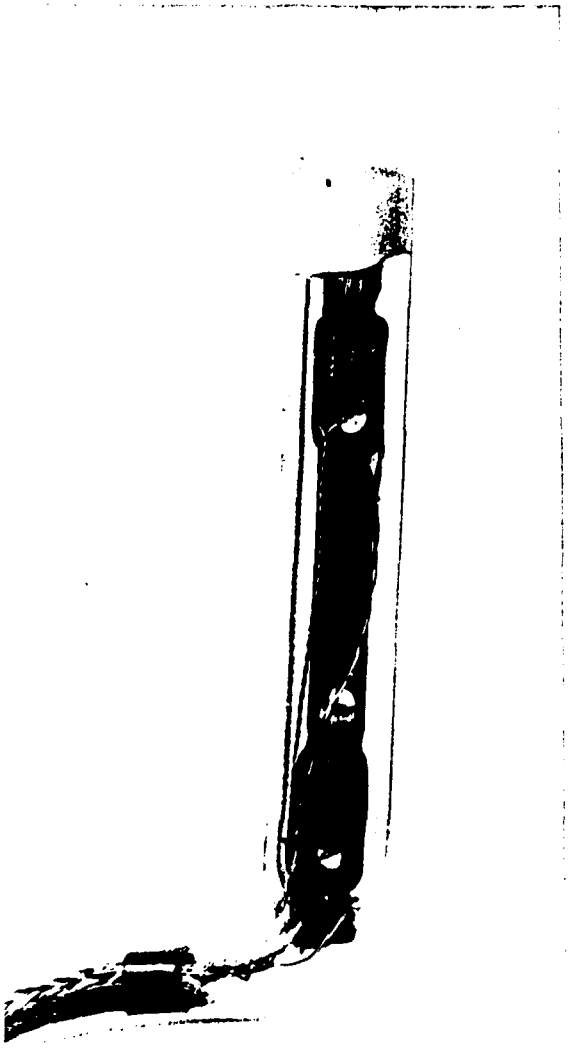

Fig.2

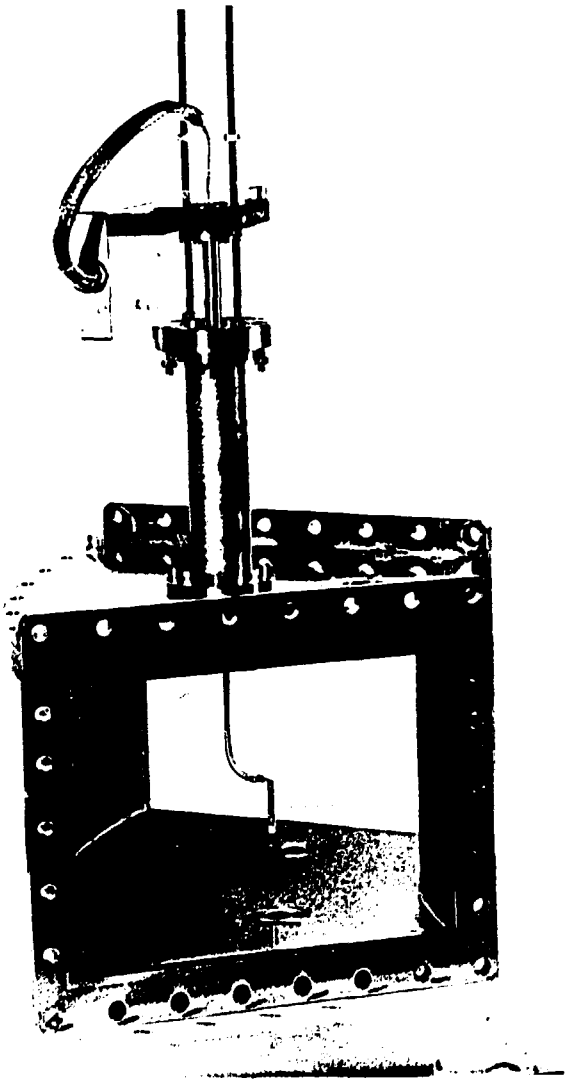

3-Dimensional Magnetic Probe.

Fig.3

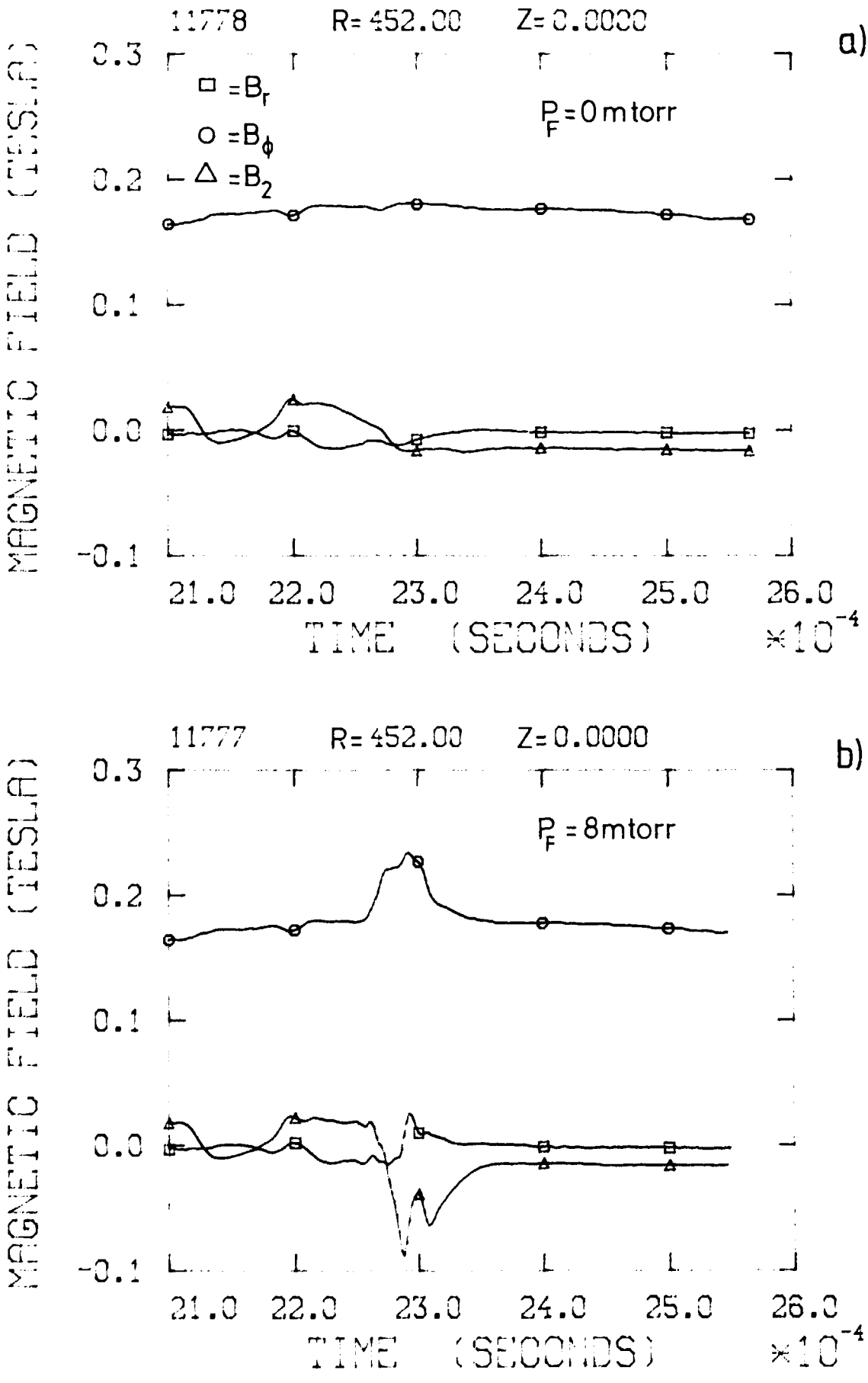
a)
11778
R= 452.00
Z= 0.0000
□ =B_r
○ =B_φ
△ =B_2
P_F = 0 m torr
0.3
0.2
0.1
0.0
-0.1
MAGNETIC FIELD (TESLA)
21.0
22.0
23.0
24.0
25.0
26.0
TIME (SECONDS)
×10^-4
b)
11777
R= 452.00
Z= 0.0000
P_F = 8 m torr
0.3
0.2
0.1
0.0
-0.1
MAGNETIC FIELD (TESLA)
21.0
22.0
23.0
24.0
25.0
26.0
TIME (SECONDS)
×10^-4

Fig. 4

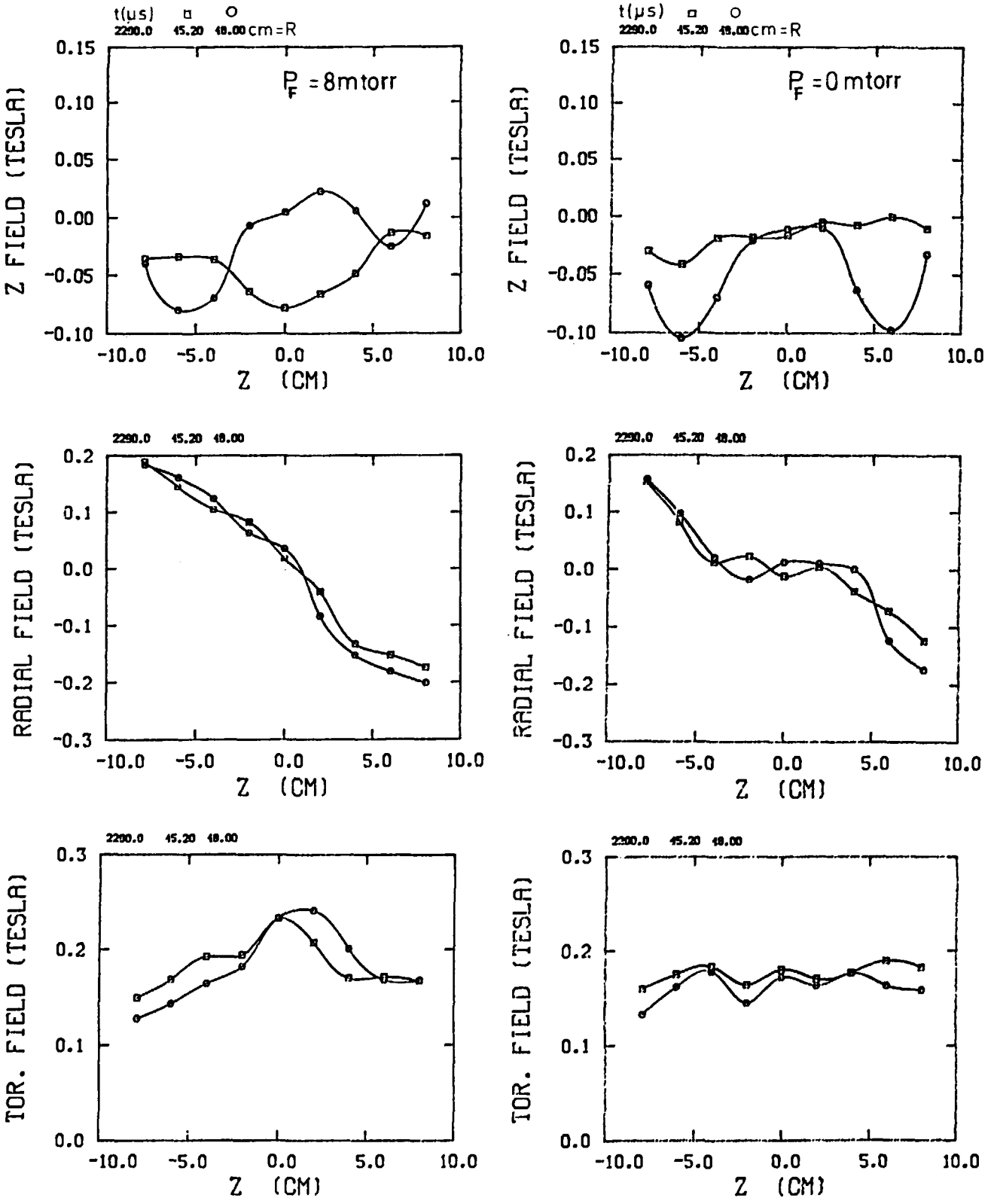

VERTICAL PROFILES

Fig.5

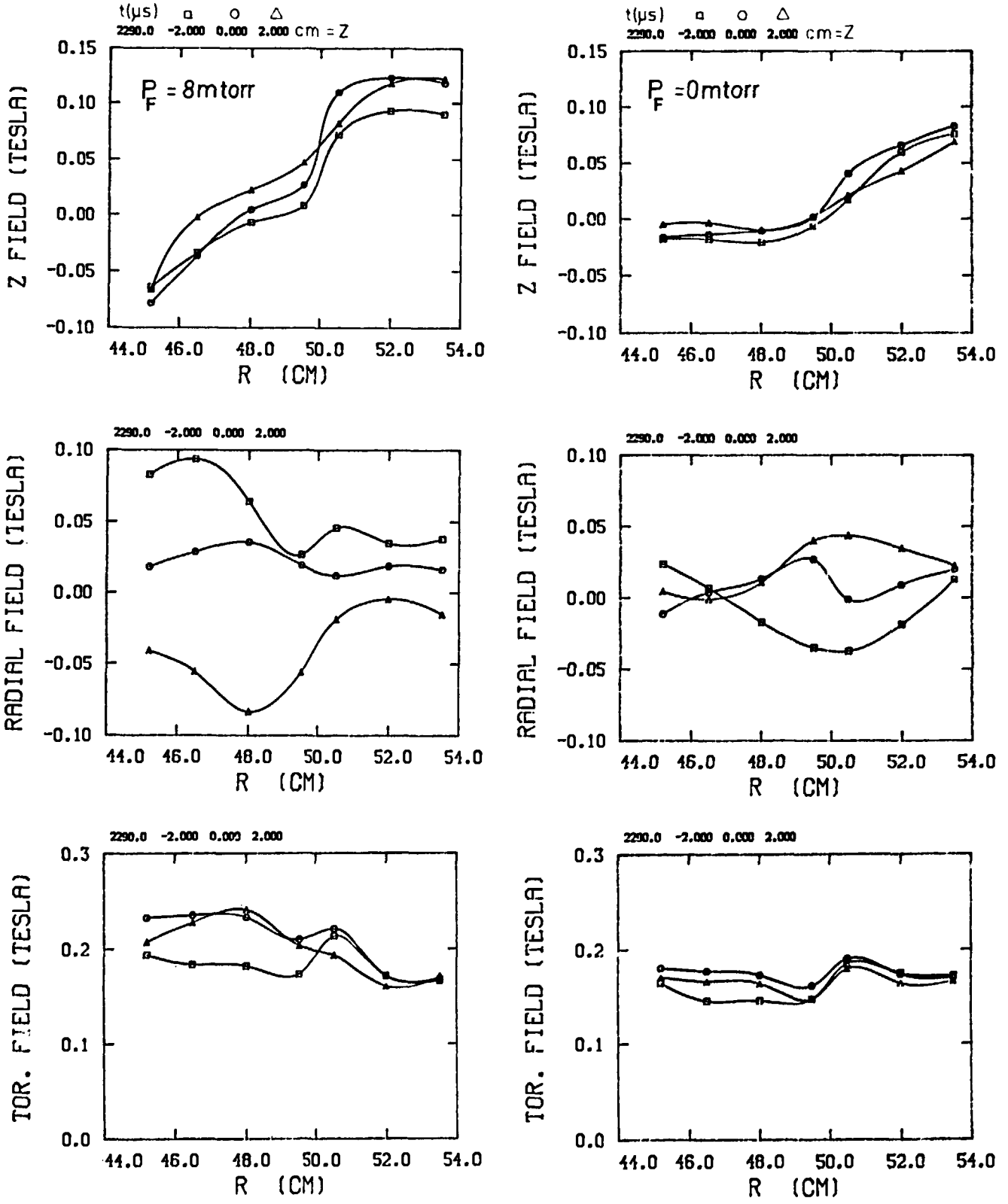

RADIAL PROFILES

Fig.6

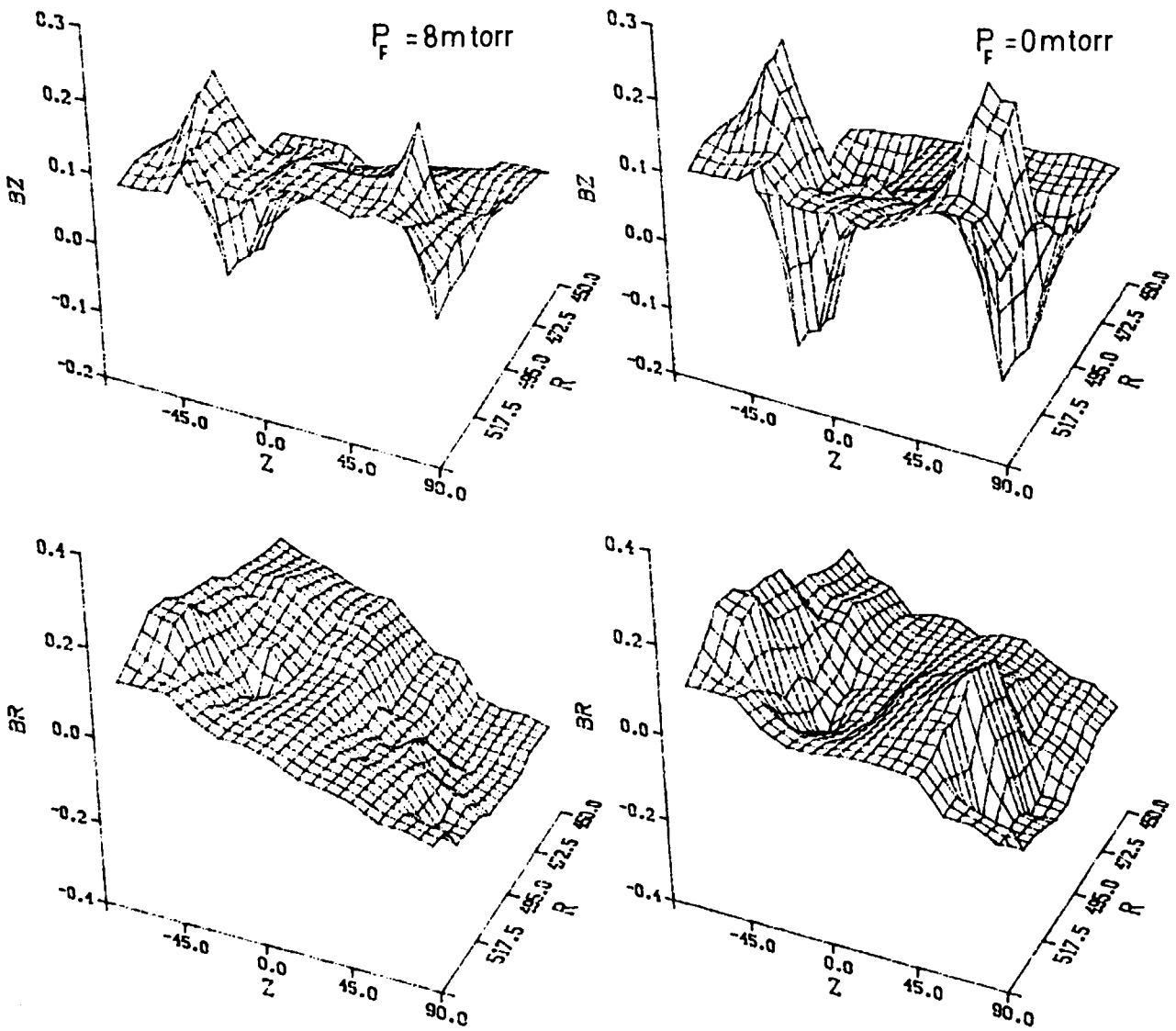

3-D MAGNETIC FIELD PROFILES

INVERSE FIELD STRENGTH PLOT

Fig.7

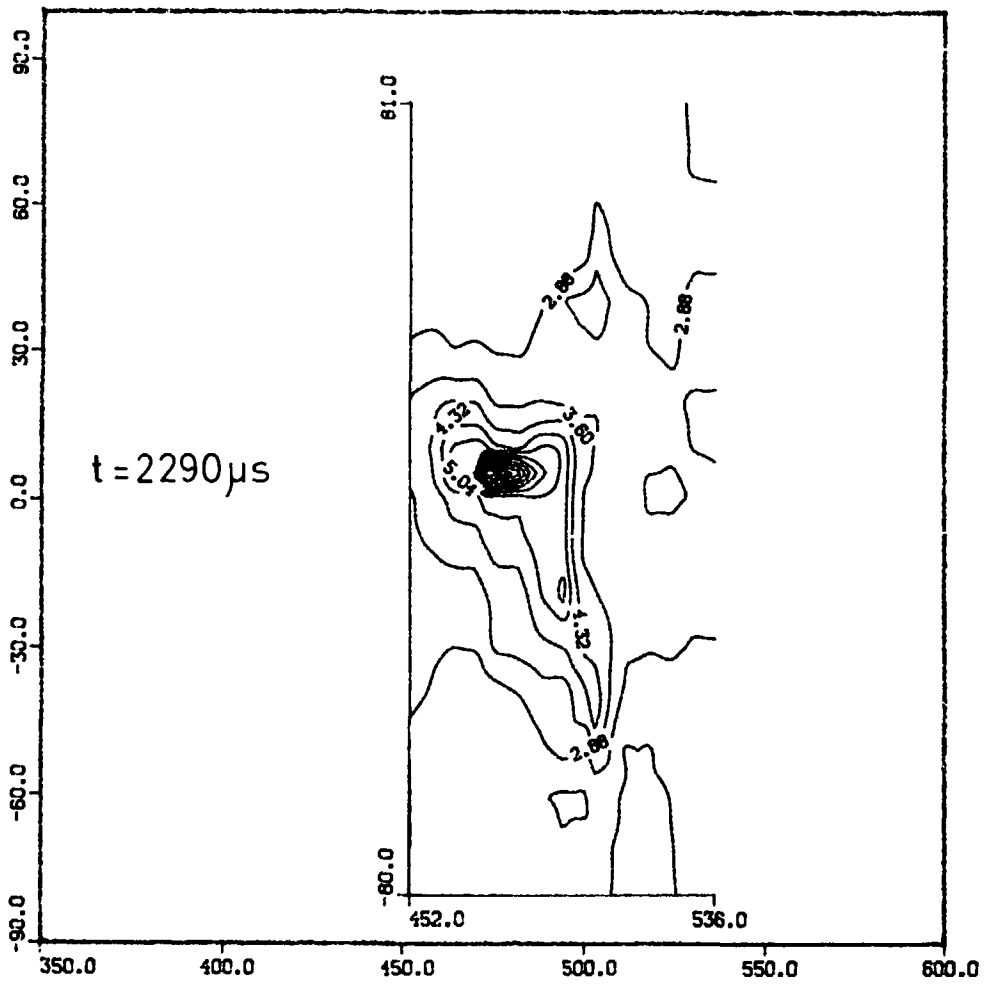

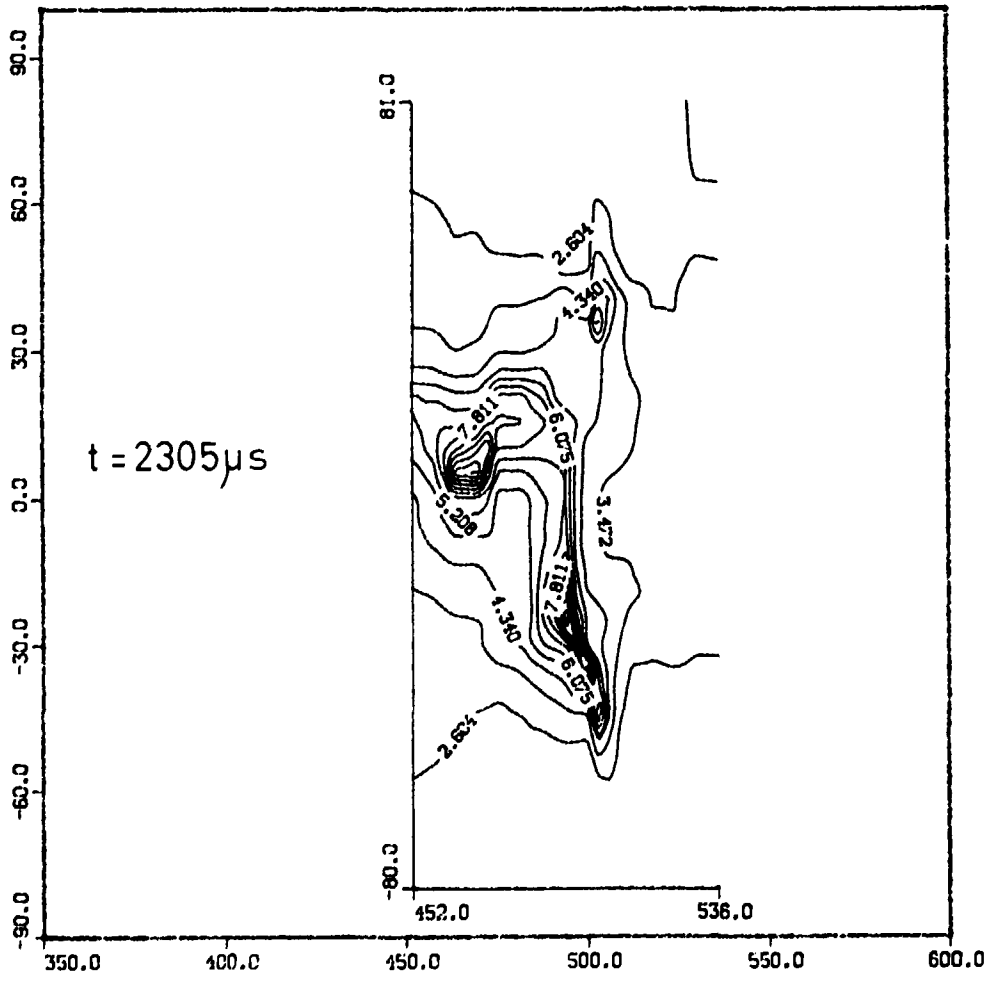

Fig.8

EXPERIMENTAL

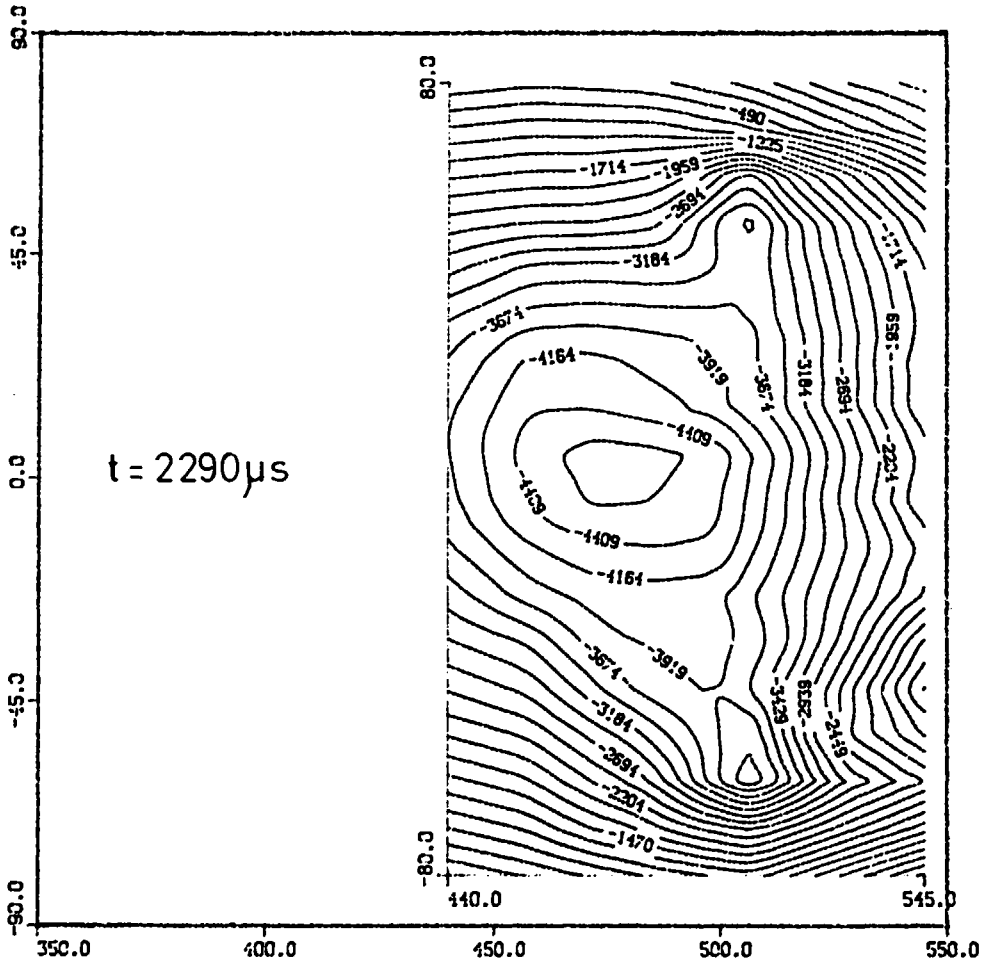

ANALYTICAL

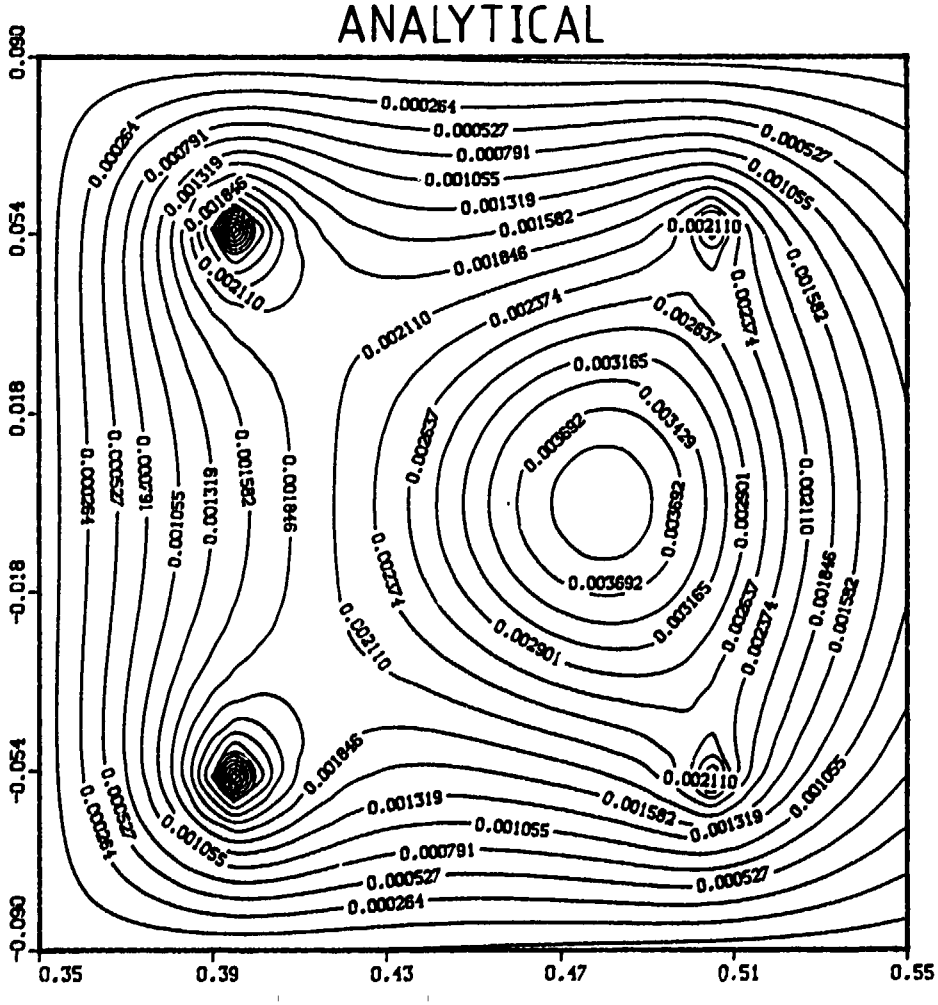

Fig. 9

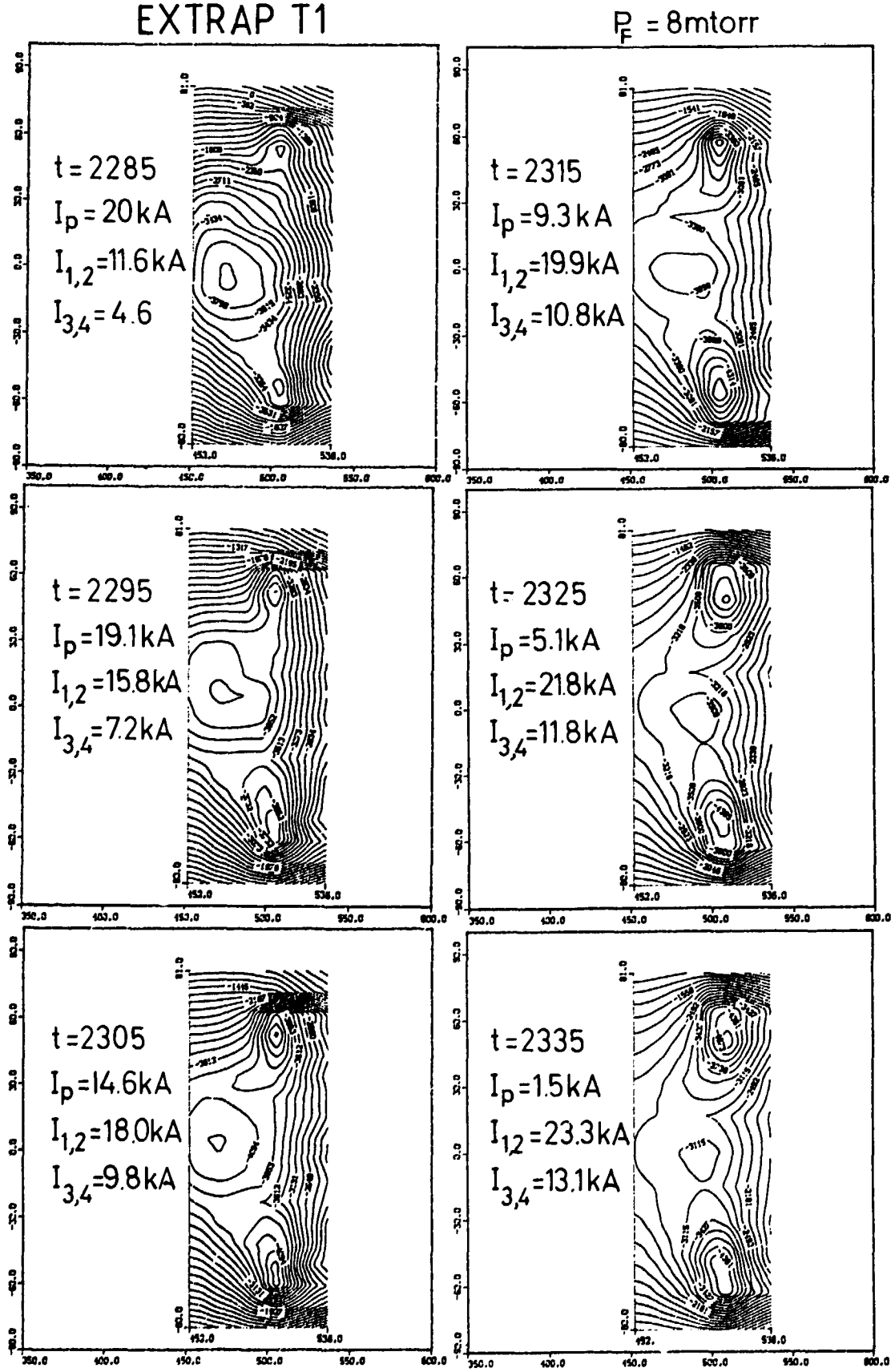
EXTRAP T1
P_F = 8mtorr
t = 2285
I_p = 20kA
$I_{1,2}$ = 11.6kA
$I_{3,4}$ = 4.6
t = 2315
I_p = 9.3kA
$I_{1,2}$ = 19.9kA
$I_{3,4}$ = 10.8kA
t = 2295
I_p = 19.1kA
$I_{1,2}$ = 15.8kA
$I_{3,4}$ = 7.2kA
t = 2325
I_p = 5.1kA
$I_{1,2}$ = 21.8kA
$I_{3,4}$ = 11.8kA
t = 2305
I_p = 14.6kA
$I_{1,2}$ = 18.0kA
$I_{3,4}$ = 9.8kA
t = 2335
I_p = 1.5kA
$I_{1,2}$ = 23.3kA
$I_{3,4}$ = 13.1kA

Fig.10

Magnetic axis position vs. time.

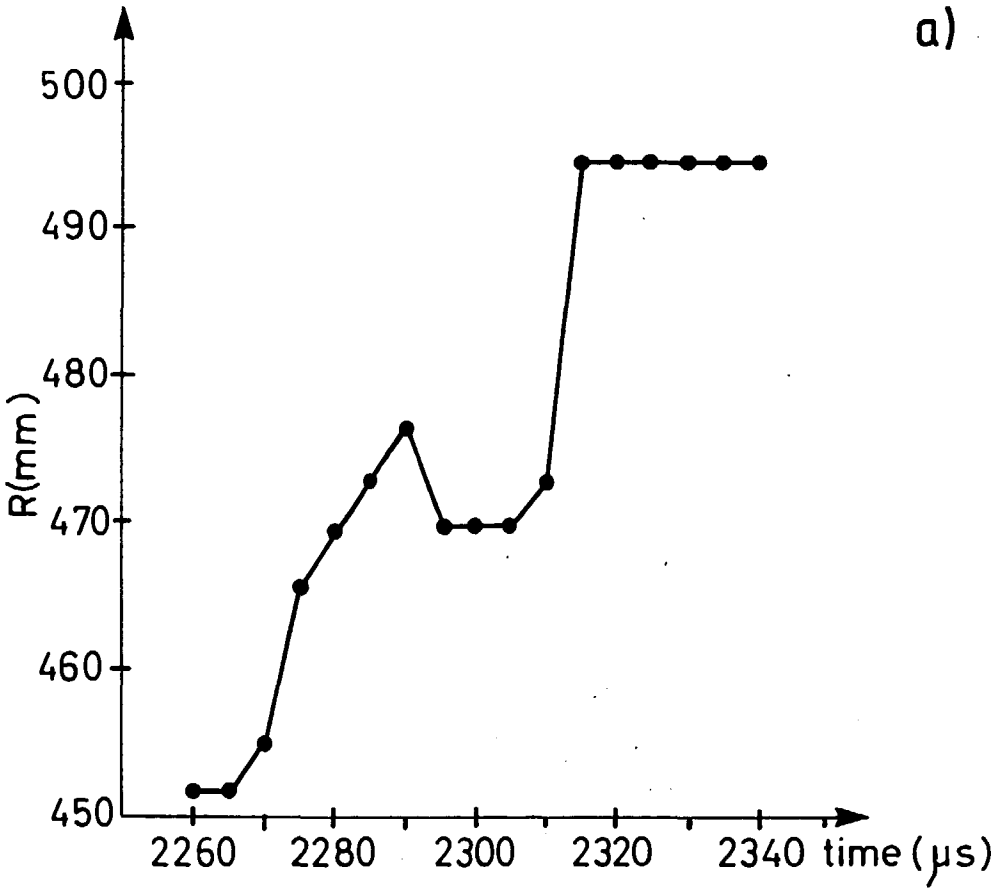

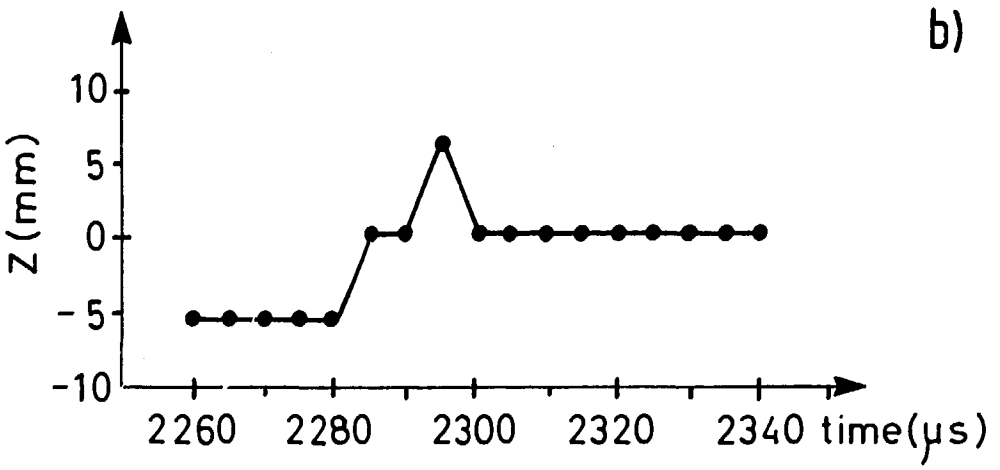

Fig.11

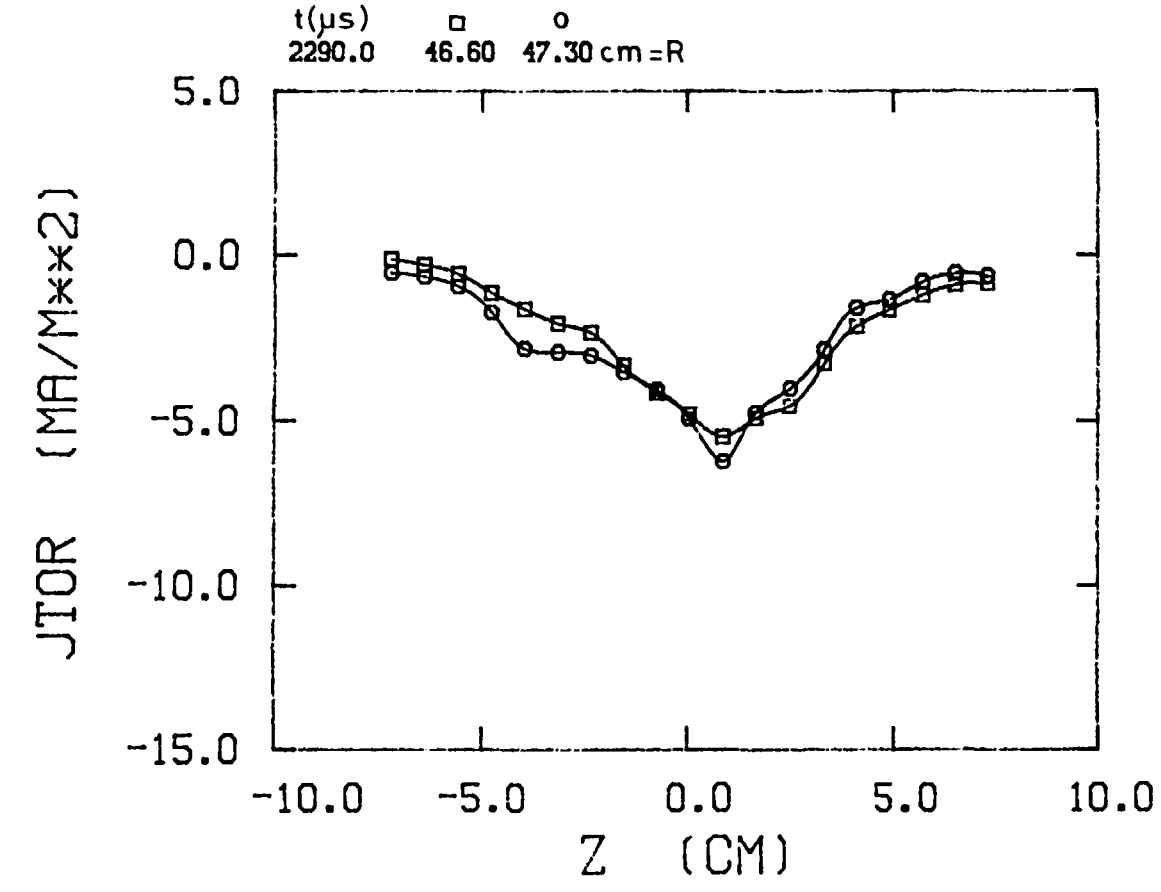
t(μs) □ o
2290.0 46.60 47.30 cm =R
5.0
0.0
-5.0
-10.0
-15.0
JTOR (MA/M**2)
-10.0 -5.0 0.0 5.0 10.0
Z (CM)

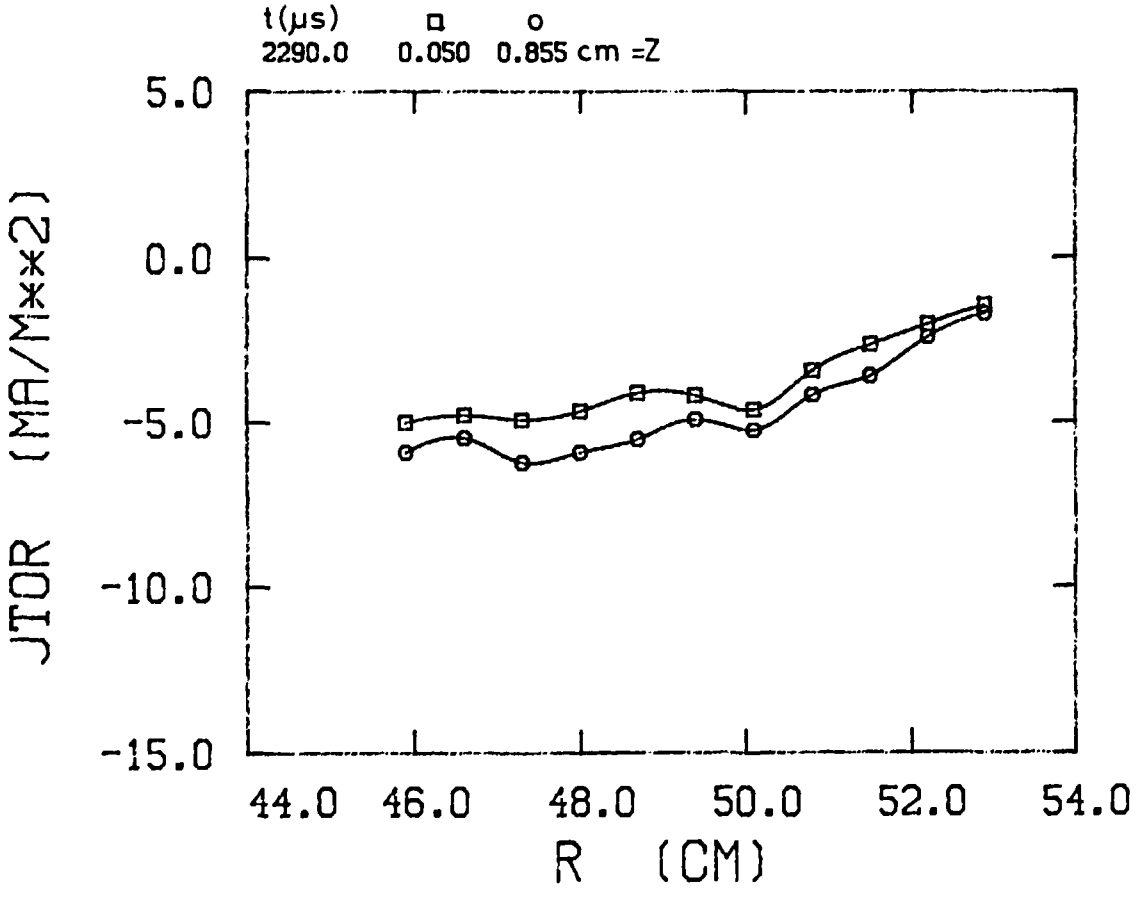
t(μs) □ o
2290.0 0.050 0.855 cm =Z
5.0
0.0
-5.0
-10.0
-15.0
JTOR (MA/M**2)
44.0 46.0 48.0 50.0 52.0 54.0
R (CM)

Fig.12

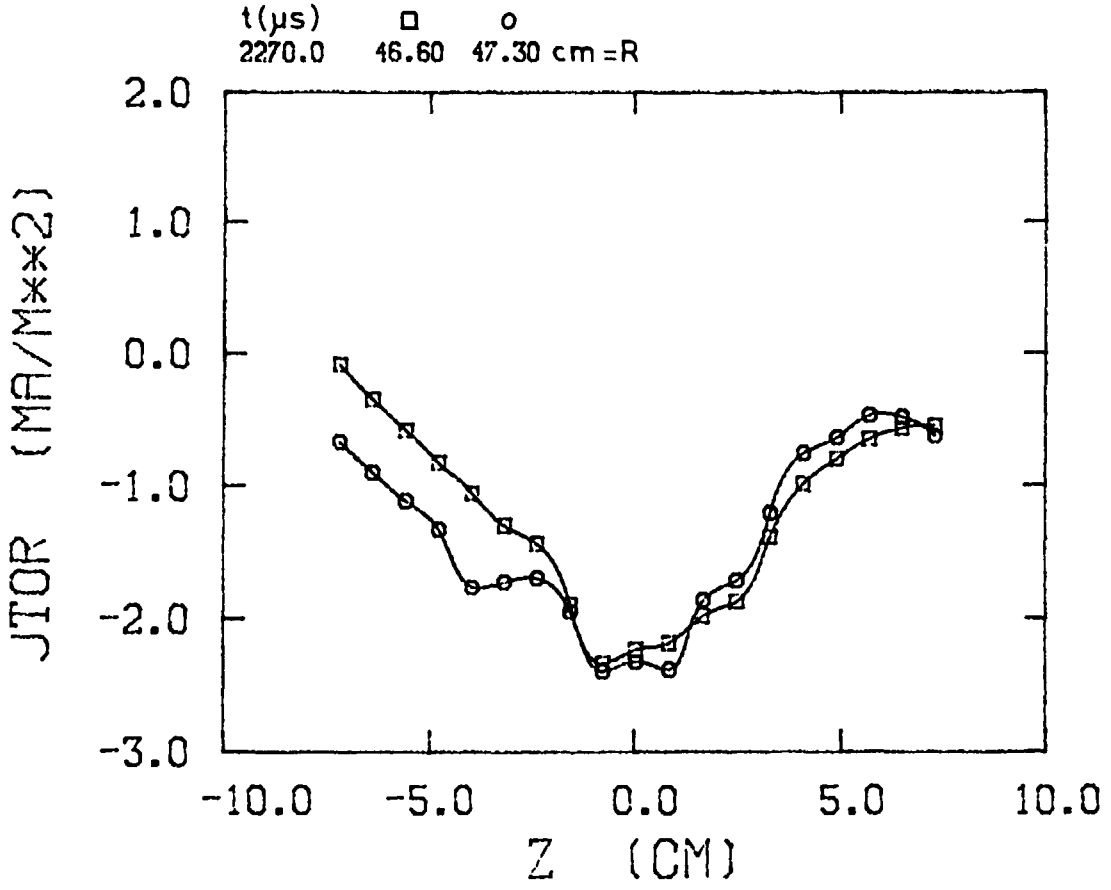
t(μs) □ o
2270.0 46.60 47.30 cm=R
JTOR (MA/M**2)
2.0
1.0
0.0
-1.0
-2.0
-3.0
-10.0
-5.0
0.0
5.0
10.0
Z (CM)

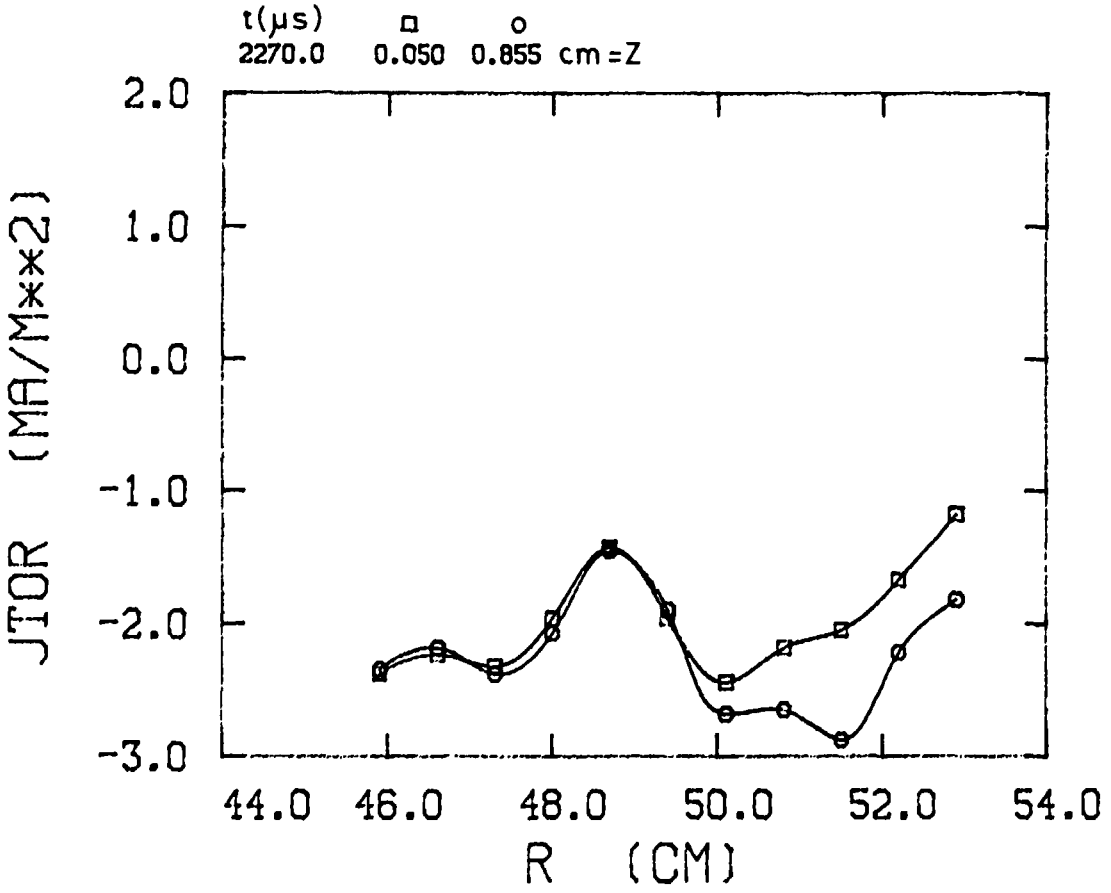
t(μs) □ o
2270.0 0.050 0.855 cm=Z
JTOR (MA/M**2)
2.0
1.0
0.0
-1.0
-2.0
-3.0
44.0
46.0
48.0
50.0
52.0
54.0
R (CM)

Magnetic Field Profiles $P_F = 4$ mtorr

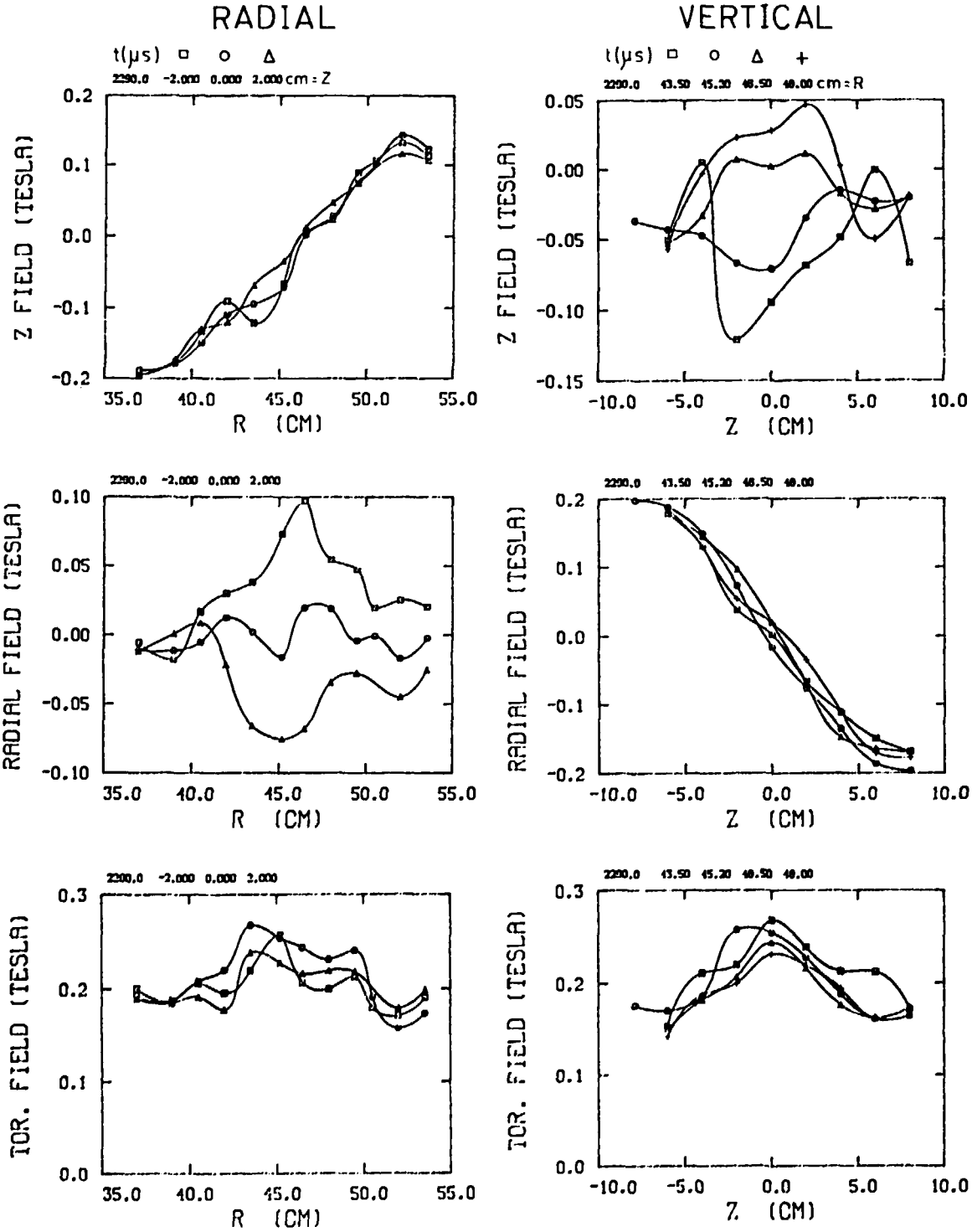

Fig.14

EXTRAP T-1 Inverse field strength plots $P_F = 4$ mTorr

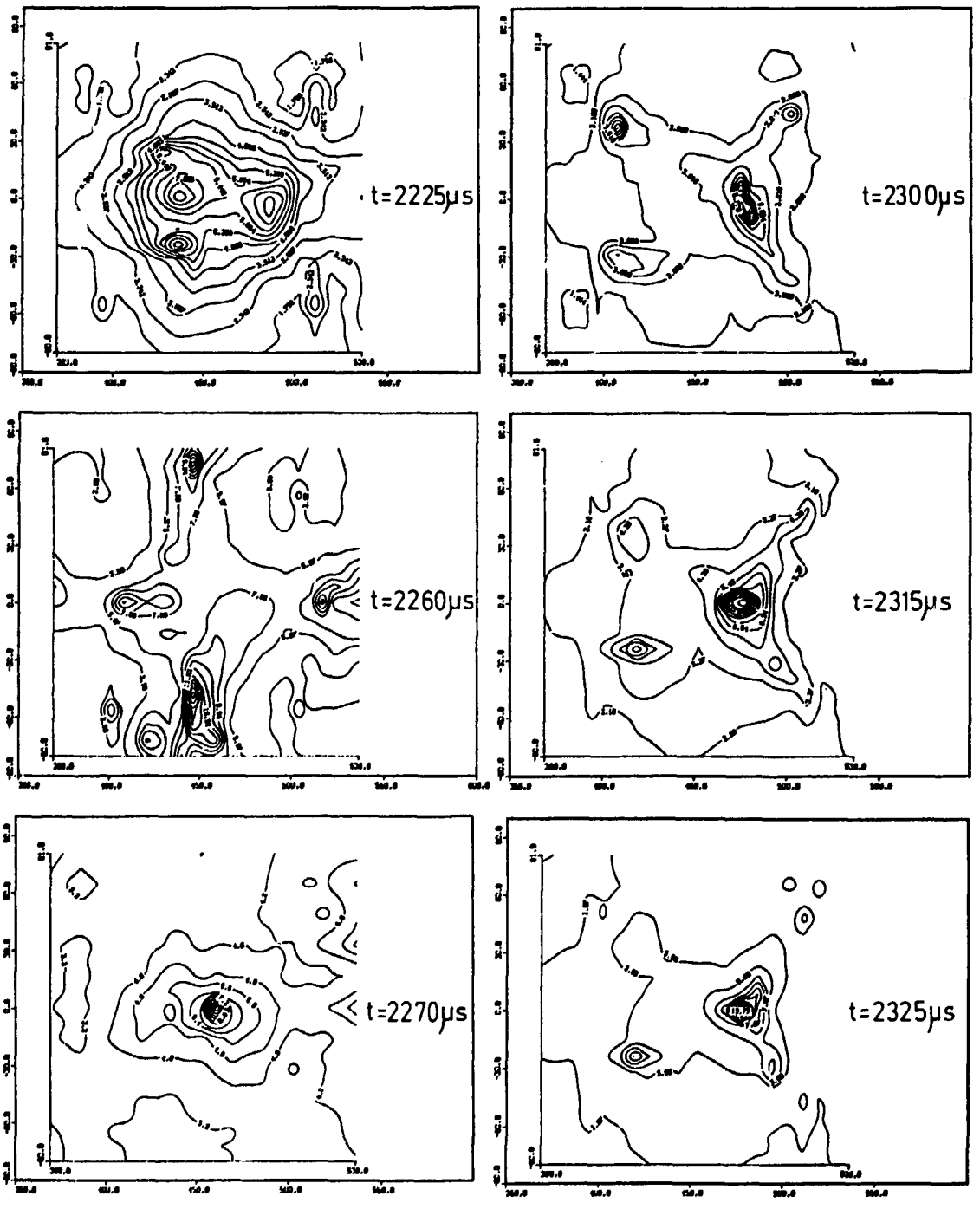

Fig.15

EXTRAP T-1 Magnetic flux surfaces $P_F = 4\,mTorr$

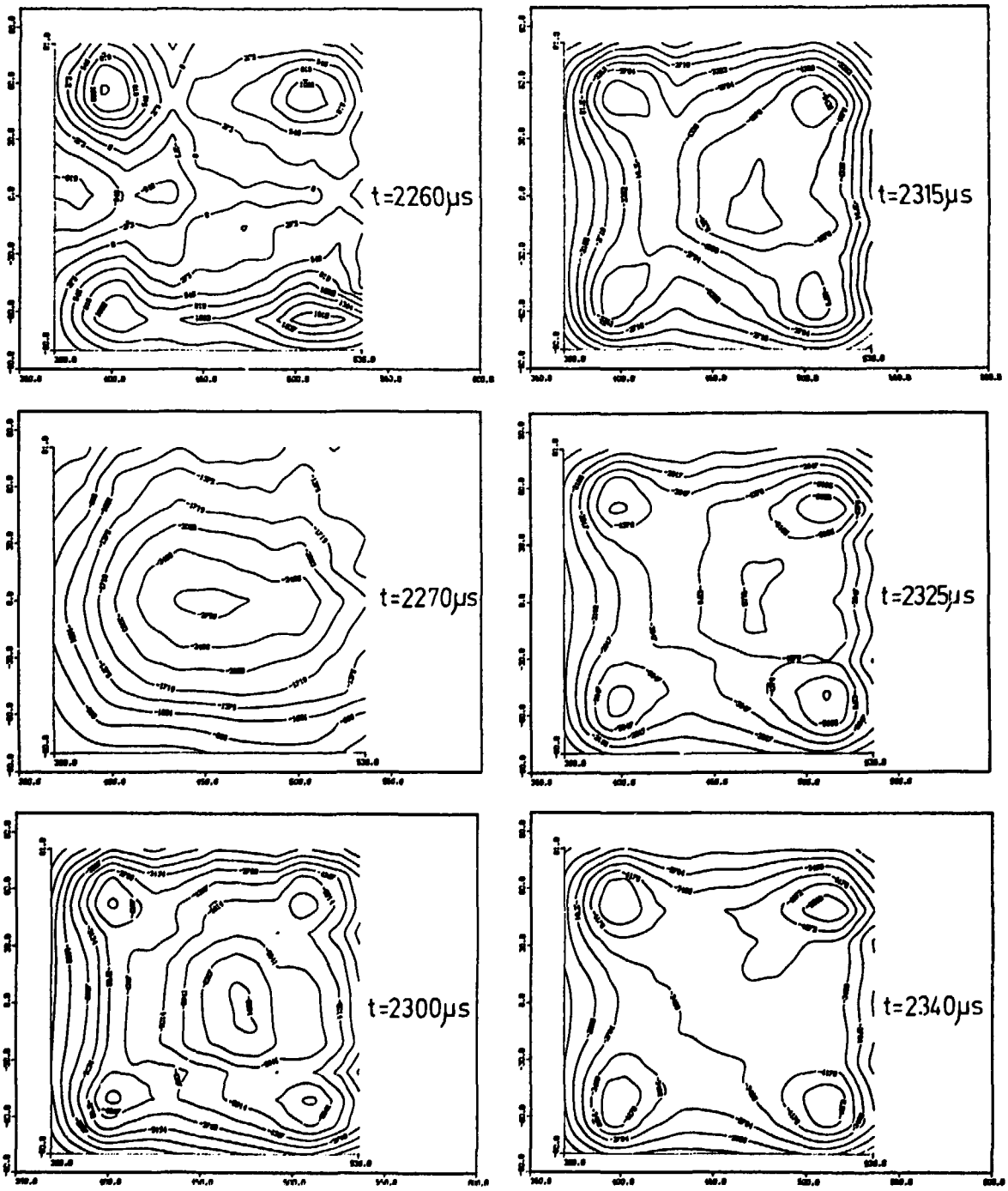

Fig.16

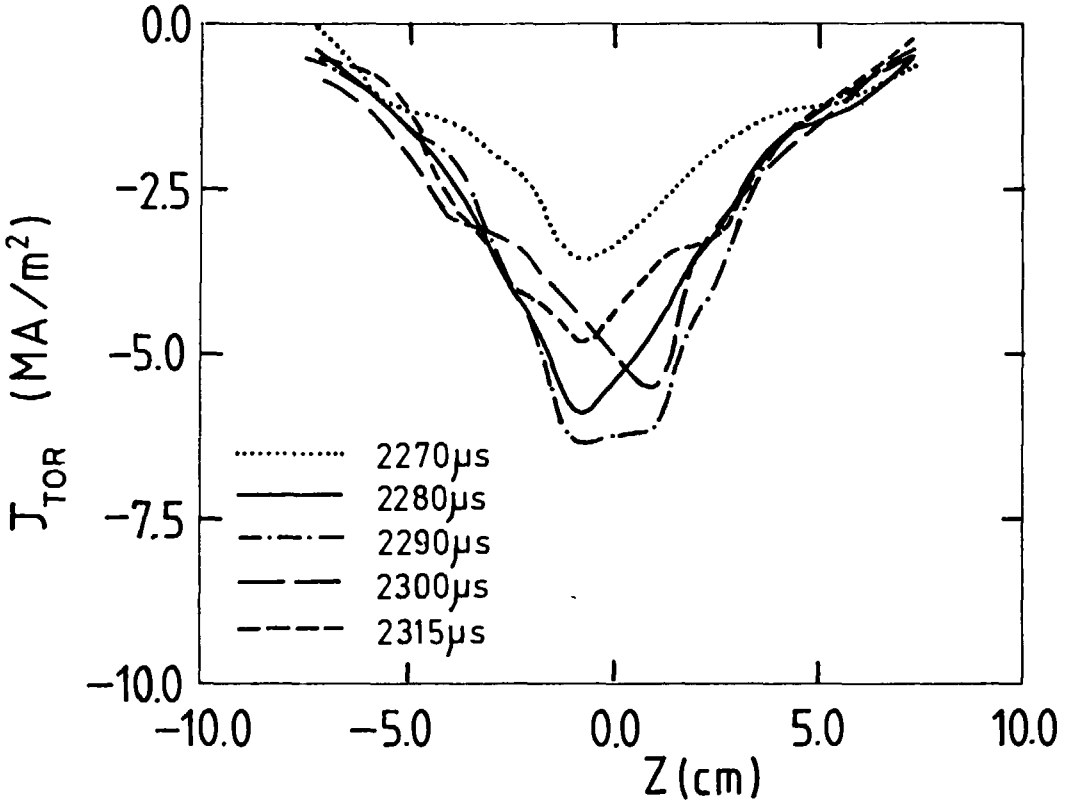
0.0
-2.5
-5.0
-7.5
-10.0
J_{TOR} (MA/m²)
2270μs
2280μs
2290μs
2300μs
2315μs
-10.0
-5.0
0.0
5.0
10.0
Z (cm)

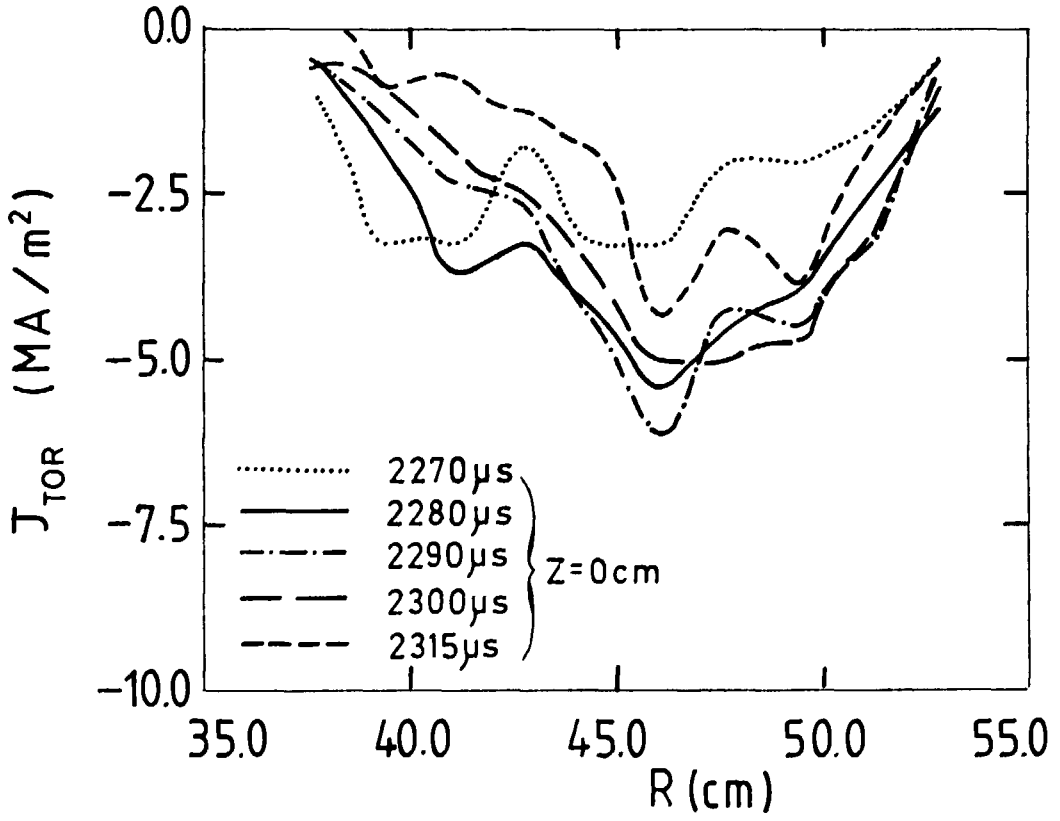
0.0
-2.5
-5.0
-7.5
-10.0
J_{TOR} (MA/m²)
2270μs
2280μs
2290μs
2300μs
2315μs
Z=0cm
35.0
40.0
45.0
50.0
55.0
R (cm)

Fig.17

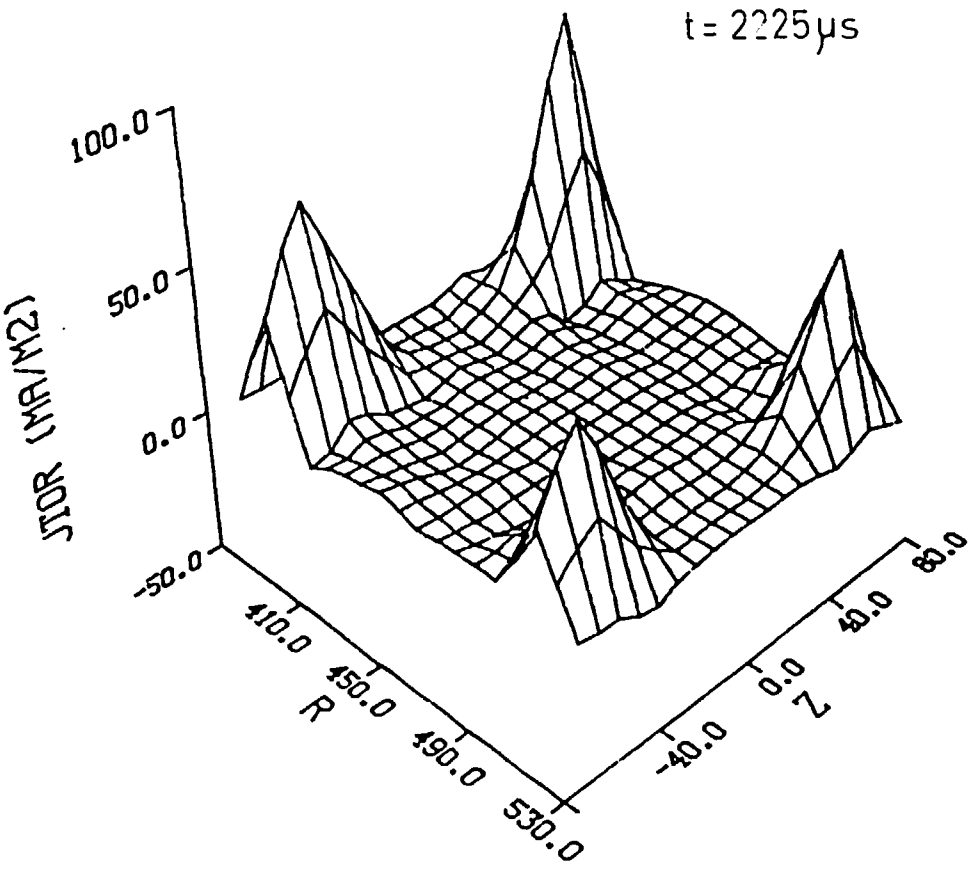
t = 2225μs
100.0
50.0
0.0
-50.0
JTOR (MA/M2)
410.0
450.0
490.0
530.0
R
-40.0
0.0
40.0
80.0
Z

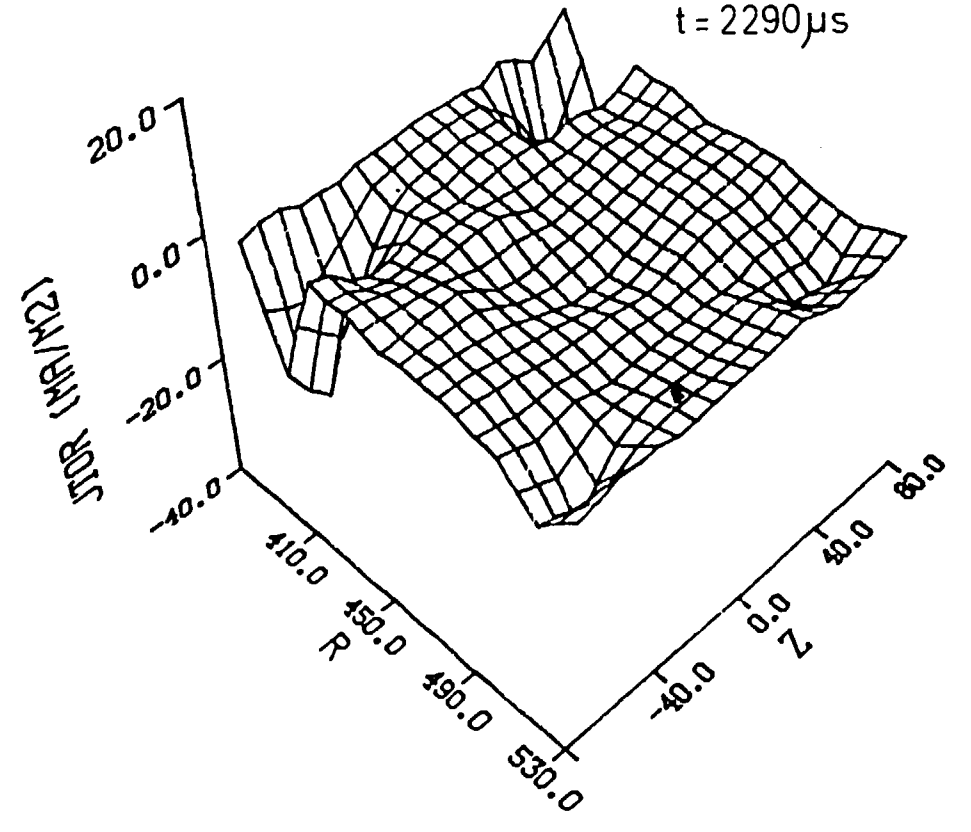
t = 2290μs
20.0
0.0
-20.0
-40.0
JTOR (MA/M2)
410.0
450.0
490.0
530.0
R
-40.0
0.0
40.0
80.0
Z

STRIPLINE APPARATUS

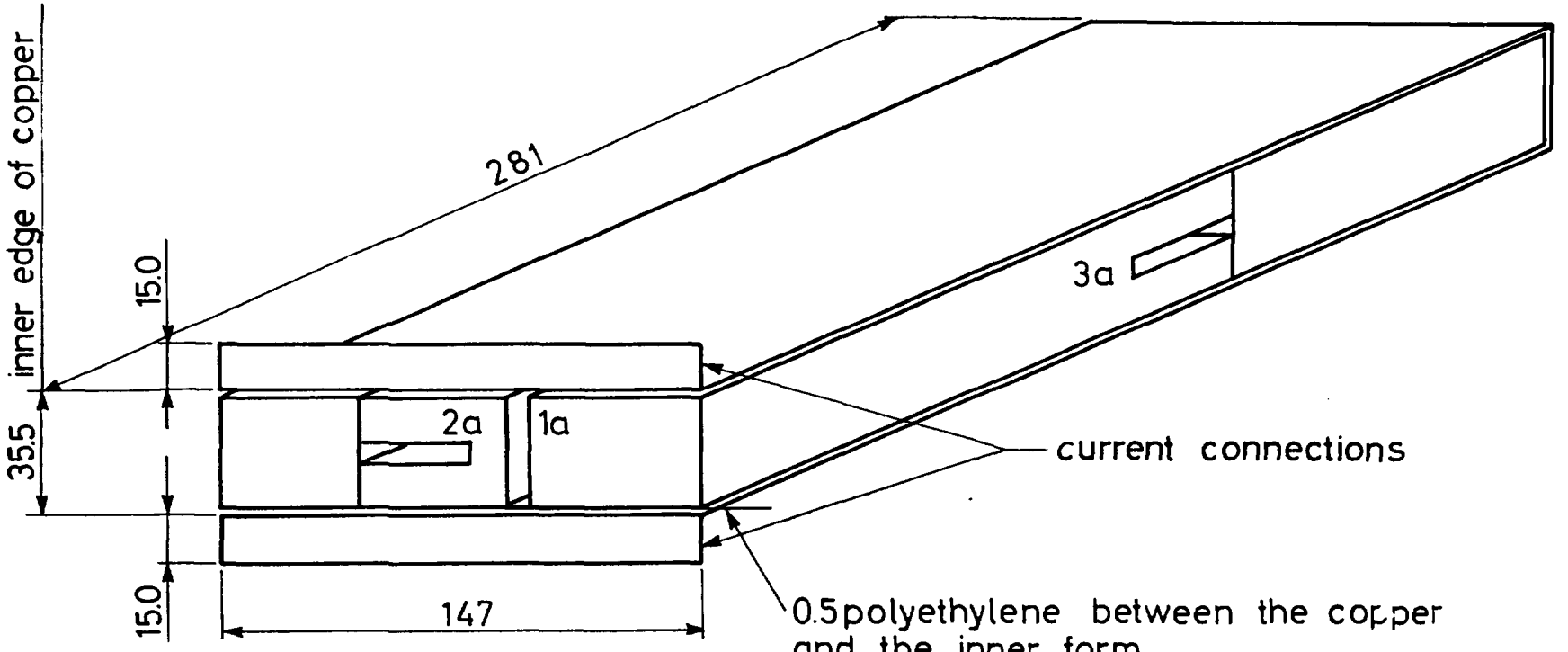

Fig.A1

Fig. A2

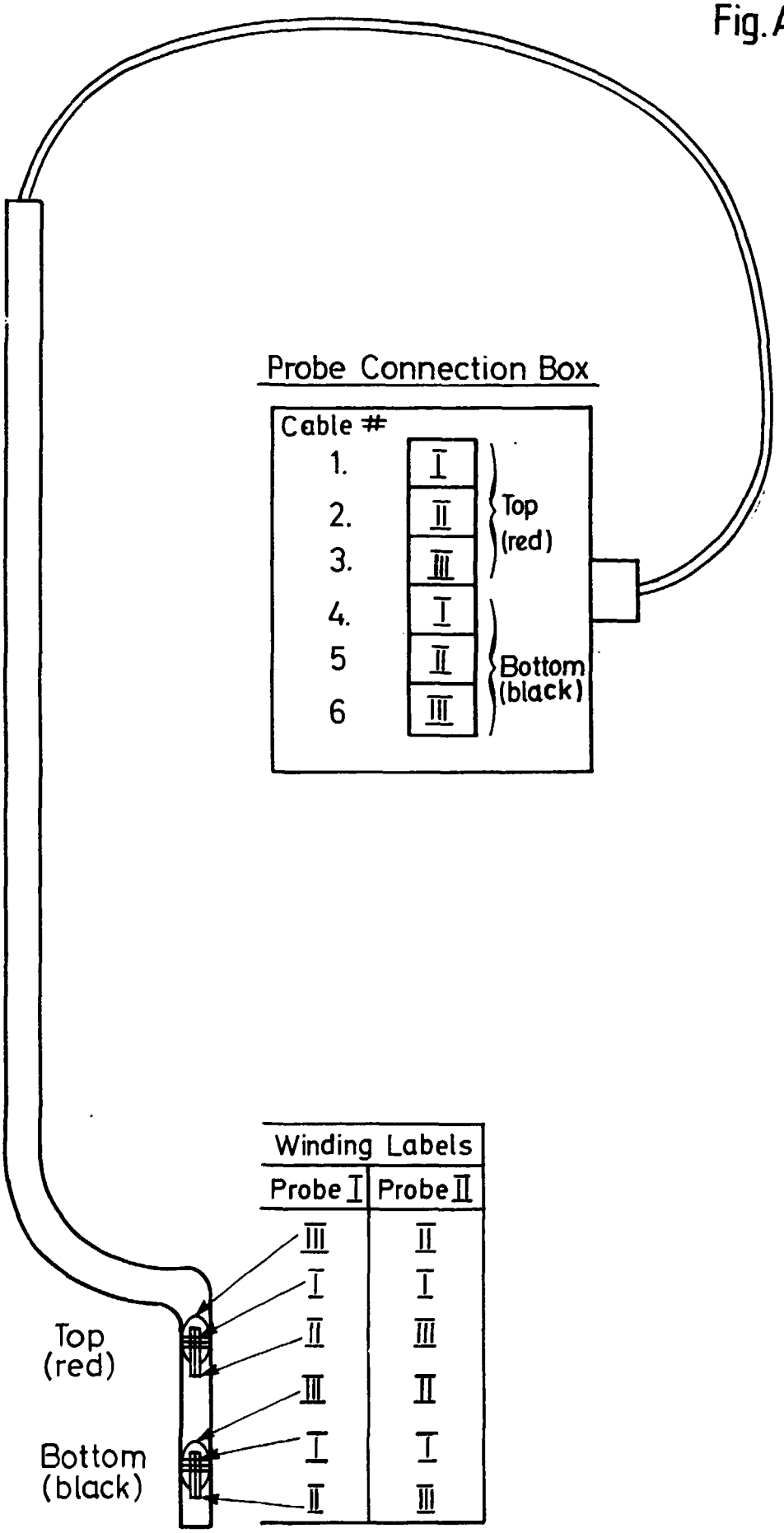
Probe Connection Box
Cable #
1.
2.
3.
4.
5
6
I
II
III
I
II
III
Top
(red)
Bottom
(black)
Winding Labels
Probe I
Probe II
III
I
II
III
I
II
II
I
III
II
I
III
Top
(red)
Bottom
(black)

Fig.A3

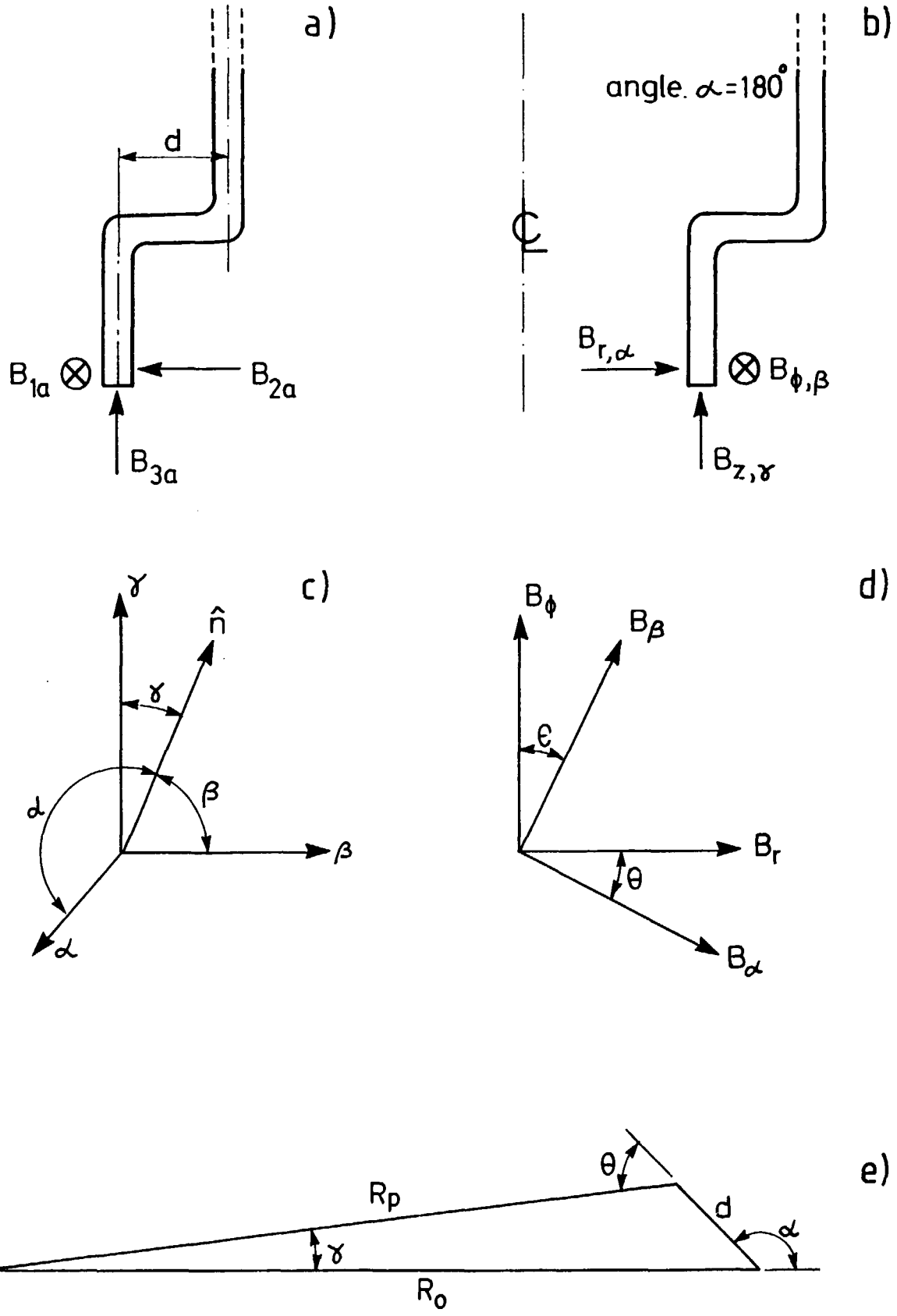
a)
d
B_{1a}
B_{2a}
B_{3a}
b)
angle. $\alpha = 180°$
$B_{r,\alpha}$
$B_{\phi,\beta}$
$B_{z,\gamma}$
c)
γ
$\hat{n}$
γ
β
α
β
α
d)
B_ϕ
B_β
ϵ
B_r
θ
B_α
e)
θ
R_p
d
α
γ
R_o

TRITA-PFU-88-12

Royal Institute of Technology, Department of Plasma Physics and Fusion Research, Stockholm, Sweden

THREE-DIMENSIONAL MAGNETIC PROBE MEASUREMENTS OF EXTRAP T1 EQUILIBRIA

Eric R. Hedin, December 1988, 26 p. in English

Internal probes are described for use in measuring the three orthogonal components of the magnetic field in the Extrap T1 device. The data analysis process for numerical processing of the probe signals is also explained. Results include radial and vertical profiles of the field components, three-dimensional field plots, inverse field strength contours, two-dimensional magnetic flux plots, and toroidal current profiles.

Key words: Magnetic plasma confinement, high beta, z-pinch, Extrap, magnetic flux plots, three-dime. onal magnetic probes